# EARTHING ELECTRODES - POWER FREQUENCY AND IMPULSE BEHAVIOUR

DAN MORDECHAI EYTANI

A project report submitted to the Faculty of Engineering, University of the Witwatersrand, in partial fulfilment of the requirements for the degree of Master of Science in Engineering.

Johannesburg, 1995

**DECLARATION**

I declare that this project report is my own work, the assistance which I have received is as follows:
Assistance in construction of electrolytic tank and measurements in it.
Construction of the test set-up at NETFA
HV measurements at NETFA
assistance with step potential measurements
Assistance in typing and printing this report
This project report is being submitted for the Degree of Master of Science in Engineering in the University of the Witwatersrand, Johannesburg. It has not been submitted before for any degree or examination in any other university.

D Eytani

Dan Mordechai Eytani

19th day of April 1995

**ABSTRACT**

Power frequency and Impulse tests were performed on earth electrodes, which are being used in MV networks. The electrodes are combinations of conductors buried in a trench and earth rods, which are driven vertically into the ground.

The power frequency tests included measurements of apparent electrode resistances and measurements of the surface equipotentials in the proximity of electrodes while they were carrying fault current. It was found that in an area where the soil resistivity is decreasing with depth the use of long rods reduced the low frequency electrode resistance significantly. Step potentials around the electrodes were quantified.

The impulse current distribution in the electrodes was measured and it was found that most of the current is dissipated from the rods. The reduction in electrode resistance under impulse conditions was quantified for soil with resistivity of a few hundred ohms in the top layer dropping to 150-200 ohms at depth of 3 meters.

The study provides a better understanding of the principles which should be applied in the design of earth electrodes.

TO MY PARENTS

RUTH AND SHMUEL EYTANI

WITH LOVE

**ACKNOWLEDGEMENT**

I would like to thank W Glynn and A Bekker (Johannesburg distributor - ESKOM) for providing the funds and allowing the time spent on this project.

I would like to thank the following people for their contribution towards this project:
A Abrosie - Technology section JHB distributor
H Fellows - Wits HV Laboratory
T Jacobs - Wits HV Laboratory
M Meyer - Technology section JHB distributor
A Muscat - Wits
H Pinnar - HV measurements, TRI
M Roberts - HV measurements, TRI
M Van Rensburg - HV Laboratory, SABS
G Whyte - Technology section JHB distributor

Finally I would like to thank my supervisor Dr J Van Coller for his sound technical advice and guidance.

CONTENTS PAGE

CONTENTS PAGE

## LIST OF SYMBOLS

| | |
|---|---|
| d | wire diameter, m. |
| h | buried depth of conductor, m. |
| k | empirical constant ( in body current calculation) |
| l | rod length, m. |
| r | apparent electrode radius, m. |
| $r_{cm}$ | maximum apparent conductor radius, m. |
| $r_o$ | electrode conductor radius, m. |
| s | characteristic distance from center of electrode to the outermost point, m. |
| t | time, s. |
| $t_s$ | duration of current exposure, s. |
| $\rho$ | soil resistivity, $\Omega$ m . |
| $\rho_0$ | low current soil resistivity, $\Omega$ m . |
| $\tau_1$ | ionization time constant, s. |
| $\tau_2$ | deionization time constant, s. |
| A | electrode surface area, $m^2$. |
| $E_C$ | critical electrical field, kV/m. |
| $E_{STEP}$ | step potential |
| $E_{TOUCH}$ | touch potential |
| G | ground conductance per unit length, $1/\Omega$ m . |
| I | current, A. |
| $I_B$ | body current, A. |
| J | current density, A/ $m^2$. |
| $J_C$ | critical current density, A/ $m^2$. |
| R | resistance per unit length , $\Omega$/m . |
| $R_B$ | equivalent body resistance, $\Omega$. |
| $R_E$ | electrode resistance, $\Omega$. |
| $R_{2Fs}$ | series footing resistance, $\Omega$. |
| $R_{2Fp}$ | parallel footing resistance, $\Omega$. |
| $SF_{11}$ | scaling factor for 11kV network voltage. |
| $SF_{22}$ | scaling factor for 22kV network voltage . |
| V | voltage, v. |
| Z | conventional impedance, $\Omega$. |
| Zo | impulse impedance, $\Omega$. |

## NOMENCLATURE

**conventional impedance.** The ratio between the maximum value of the total earth electrode voltage and the peak value of the impulse current.

**ground.** A conducting connection, whether intentional or accidental, by which an electric circuit or equipment is connected to the earth.

**ground return circuit.** A circuit in which the earth or an equivalent conducting body is utilized to complete the circuit and allow current circulation from or to its current source.

**ground electrode.** A conductor imbedded in the earth and used for collecting ground current from or dissipating ground current into the earth.

**ground potential rise (GPR).** The maximum voltage that an earth electrode may attain relative to a distant grounding point assumed to be at the potential of remote earth.

**impulse impedance.** The ratio between the instantaneous values of the total ground voltage of an earth electrode and of the total current at the injection point.

**Rogowski coil.** An open circuited, air-cored current transformer with a resistor-capacitor (RC) integrator on the secondary side - used for measurements of very high currents.

**step potential.** The difference in surface potential experienced by a person bridging a distance of 1 m with his feet without contacting any other grounded object.

**touch voltage.** The potential difference between the ground potential rise(GPR) and the surface potential at the point where person is standing, while at the same time having his hands in contact with a grounded structure.

**transferred voltage.** A special case of the touch voltage where a voltage is transferred out of the area of the earth electrode.

## 1. INTRODUCTION

In South Africa millions of people still do not have electricity - this is the reason for the big electrification drive which is taking place throughout the country. A lot of work has been done and a lot of work is currently in progress in order to ensure that the electrification networks which will be constructed will be cost effective without compromising their performance and safety.

Earthing is one of the most important factors, which effects both the performance of the electrical network and its safety. This report deals with earth electrodes that are mainly used on medium voltage (MV) networks. Two aspects were studied:

a. Power frequency: electrode resistance to true earth which is important for correct protection operation, and surface potentials - the safety aspect.
b. Impulse behaviour: the current distribution within the electrode and the reduction in electrode resistance under impulse.

The aim of the study was to test various electrode configurations for their resistances and their surface equipotentials, as well as, their impulse behaviour - in order to get a better understanding of the principles which should be applied in the design of earth electrodes.

This report considers two behaviours - the power frequency and the impulse behaviour. This introductory chapter includes two sections:

Section 1.1 gives the background on the safety aspects of earthing regarding the permissible body currents, step and touch potentials, as well as a short review of the experimental work that was done in this field.

Section 1.2 gives the background on impulse behaviour of earthing electrodes. The classification of localized earth electrodes and extended earth electrodes is explained, as well as the electrical breakdown and ionization processes in the soil. Dynamic models of localized and extended earth electrodes are presented.

Chapter 2 covers the power frequency measurements and includes the experimental set-up and testing procedure. The step potential field measurements and the electrolytic tank measurements are presented and interpreted, followed by a discussion of the results.

Chapter 3 covers the impulse behaviour and includes the experimental set-up and testing procedure. The results for current distribution and reduction in electrode resistance are presented and interpreted, followed by a discussion of the results.

Chapter 4 contains the conclusions for the work presented as well as recommendations for future work to be done.

## 1.1 Earth electrodes - Power Frequency

### 1.1.1 Safety in earthing

The main reference for this section is the: IEEE Guide for safety in AC Substation Grounding [1].

**Permissible body current limit**

When current is passing through the human body its effects depend on the duration, magnitude, and frequency of this current. The most dangerous consequence is heart fibrillation, resulting in immediate arrest of blood circulation.

Effect of frequency - It was found that humans are very vulnerable to currents at power frequencies, however at higher frequencies the body can tolerate much higher currents. The same applies to very low frequencies and DC.

Effects of magnitude and duration - The duration for which most people can tolerate power frequency current, without going into heart fibrillation is related to its magnitude by Dalziel's equation:

$$I_B = k / \sqrt{t_s} \qquad \text{(Eq 1)}$$

Where

$I_B$ - rms magnitude of the current through the body
$k$ - empirical constant ( $k = 0.116$ for a person weighing 50Kg )
$t_s$ - duration of current exposure in s

The equation above is valid for the time range of 0.03 - 3 s. The value of 100mA was suggested as the fibrillation threshold if shock durations are not specified.

**Step and Touch voltage criteria**

Resistance of the human body - The resistance of the internal body tissues, not including skin, is approximately 300Ω . Values in the range 500- 3000Ω for body resistance including skin have been suggested. However, for body currents calculation a value of $R_B$ = 1000Ω is assumed and the hand and shoe contact resistances are assumed to be equal to zero.

Current paths through the body - When a person is subjected to *step* potentials, the current is enters the body in one foot and leaves it through the other foot - therefore the circuit comprises the body resistance $R_B$ in series with a series combination of the footing resistance $R_{2Fs}$ (resistance of the ground just beneath the feet). The circuit equivalent for *touch* potentials comprises $R_B$ in series with the parallel combination of $R_{2Fp}$ ( the current is flowing through both feet in parallel).
It was found that much higher foot to foot than hand to foot currents had to be used to produce the same current in the heart region.

In order to prevent heart fibrillation the maximum *step* voltage must not exceed the limit below:

$$E_{step} = (R_{2Fs} + R_B)\, I_B \qquad \text{(Eq 2)}$$

For touch voltage the limit is:

$$E_{touch} = (R_{2Fp} + R_B)\, I_B \qquad \text{(Eq 3)}$$

The footing resistances strongly depend on the soil resistivity and the actual contact between the ground and the foot.

**Evaluation of step and touch potentials**

In principle safe grounding design has two objectives [1]:
a) To provide means to carry the electric current into earth under fault conditions without exceeding any operating and equipment limits or adversely affecting continuity of supply.
b) To assure that a person in the vicinity of grounded facilities is not exposed to the danger of critical electrical shock.
Design procedures for grounding systems were developed with the aim to avoid dangerous step and touch voltages within a substation. The analytical techniques used have varied from those using simple hand calculations to those involving scale models [2] [4] or computer algorithms [15] [16].

In general the computer algorithms are based on modelling the individual components comprising the grounding system, forming a set of equations which describe the interaction between these components, then solving for the ground fault current flowing from each component into earth and then computing the surface potentials due to all the individual components.

The concept of using scale models and an electrolytic tank to simulate the performance of grounding grids was introduced by Koch in 1950 [Apx J, ref 1] . A number of papers have been published since the 1950s [2] . The purpose of the scale models and electrolytic tank was to determine the grid resistance and the surface potentials for a grounding.

A comprehensive research project was undertaken by EPRI in 1983, with the objective to develop an electrolytic tank to performance of HV AC station grounding grids during earth faults and to evaluate the effects of various design parameters by testing different ground grid configurations [2]. The results were compared with various computer program results. The following observations were made:

Uniform soil model

1) $R_E$ , $E_{STEP}$ and $E_{TOUCH}$ are inversely related to the length of the ground rods , the depth of the grid and the number of meshs in the grid.

2) The grid performance can be improved by the addition of horizontal conductors near the outer part of the grid.

3) Generally, additional ground rods are more effective then additional horizontal conductors.

4) The ground rod diameter has little effect on the overall grid performance.

Two layer soil model

1) $E_{STEP}$ and $E_{TOUCH}$ decrease with the addition of ground rods.

2) $R_E$ is inversely related to the top layer depth when it has the lower conductivity, and directly related to the top layer depth when it has the higher conductivity.

3) The decrease in $R_E$ due to the addition of ground rods is more significant when the soil conductivity is increasing with depth.

4) Ground rods penetrating a higher conductivity second layer of soil have more effect in reducing $R_E$ then ground rods penetrating a lower conductivity second layer of soil.

The work by different researchers, published thus far, relates to scale models of substation grids. Full scale tests are both costly and difficult to perform for such large areas ( several hundreds of square meters ). However, the size of earth electrodes used on MV networks is relatively small ( several tens of square meters ), hence full scale measurement becomes fissile.

### 1.1.2 Protection operation

When an earth fault occurs on an MV network - the resistance of the earth electrode largely determines the magnitude of fault current. Since most MV lines are protected by an inverse time-current relays the higher the fault current the faster the protection will operate and isolate the faulty circuit.

In the case where the earth electrode resistance is very high, it could be that the fault current would not exceed the relay pick-up and the faulty circuit will remain energized.

High-speed fault clearing is advantageous for safety reasons:

a. The probability of electric shock is greatly reduced by fast clearing time.

b. Both tests and experience show that the chance of severe injury or deaths is greatly reduced if the duration of the current flow through the body is very brief [1].

## 1.2 Earth electrodes - Impulse Behaviour

Experiments on the impulse behaviour of earth electrodes have shown that the impulse impedance of the electrodes is reduced from its low voltage power frequency value [7] [11] [17] [18] [19].This reduction is due to ionization of the soil around the earth electrode. Ionization starts once the current density on the surface of the electrode's conductors exceeds a certain critical value *Jc* that creates a critical electric field gradient *Ec* in the soil. Soil ionization is a nonlinear phenomenon, that depends the on electrical and geometrical parameters such as: soil resistivity, impulse current wave shape and magnitude and the shape and dimensions of the earth electrode .
Dynamic models for the evaluation of the impulse impedance and current and voltage distribution along the electrodes have been developed [7] [8] [9] [12].

### 1.2.1 Earth electrodes - Localized and Extended

The impulse behaviour of the earth electrodes can differ significantly depending on whether not the electrode length is negligible in comparison to the wave length of the impulsive current. Electrodes are classified as either localized or extended. For localized electrodes the ratio between the time necessary for an electromagnetic perturbation to cover its length and the impulse rise-time must be less then 1/5 or 1/6. In practice the steady state is reached after the electromagnetic wave inside the electrode has been reflected five or six times.
Localized electrodes are sometimes referred to as *Concentrated* electrodes. Extended electrodes are referred to as *Distributed* electrodes. The models that are used to analyze distributed electrodes are different to those for the concentrated electrodes because the propagation time of the electromagnetic wave along the distributed electrode has to be accounted for [8] [13].

### 1.2.2 Electrical breakdown and ionization process in the soil

Two models have been proposed to explain the electrical breakdown in the soil [10].

The first model suggests that breakdown occurs in the air voids between the grains of soil, where the electric field strength is enhanced by dielectric effects. Tests and measurements of the electrical breakdown characteristics of a soil sample in air and with the air in the voids replaced with $SF_6$ were done to verify this model. It was found that all the properties that are associated with arc initiation were consistently different for air and $SF_6$. The ratios of these quantities were comparable to the ratio of the electric field breakdown of air and $SF_6$ at one atmosphere.

Long time delays before breakdown were measured in the tests. This phenomena is attributed to areas in the soil, where microscopic films of water becomes very thin or discontinuous, resulting in a build-up of ions and creation of electrochemical polarization. The time required for this build-up of charge is known as the *Relaxation* time. These charges can cause electric field enhancement across some voids and once a certain critical level is exceeded breakdown will occur.
The time delays could be a complex function of the soil type, electrode material, electrode surface area and the electric field strength in the soil.

The second model proposes that breakdown is initiated when a water path in the soil is ohmicaly heated and a small part of it is vaporized. Breakdown then take place across the vaporized path.The thermal process in the water contained in the soil provides the explanation for the long delay times before breakdown.

In a series of laboratory experiments [10] a number of different soils were tested. The electric bre kdown field was found to be typically between 6 and 18 kV/cm . However, field experiments by different researchers [7] [17] [18] [19] yielded much lower breakdown values typically between 2 and 4 kV/cm.

### 1.2.3 Localized electrodes - Dynamic models

Two different dynamic models were suggested:

**Liew and Darviniza**

A dynamic model to describe the nonlinear surge current characteristics of concentrated (localized) earth electrodes has been developed by Liew and Darveniza [7].
Previous studies [17] [18] [19] had carried out surge tests on various soils and electrode configurations. Currents up to 12 kA and surge reduction factors between two and three were commonly used. For higher currents it was necessary to extrapolate values from the experimental results.
The Liew and Darveniza model overcomes these difficulties and accounts for the experimentally observed time-variant hysteresis as well as breakdown by ionization effects in the soil. A description of the model follows:
First, an assumption is made that the soil has the same resistivity in all directions.
As the surge current penetrates into the soil, some regions where the current density is greater than the critical value *Jc* ,will have resistivity less than the low frequency low current value $\rho_o$. This breakdown process is assumed to occur by time dependent diffuse growth of increasing ionization. The transition of the $\rho_o$ value to the lower state $\rho$ is given by:

$$\rho = \rho_o \exp(-t/\tau_1) \qquad \text{(Eq 4)}$$

Where $\tau_1$ is the ionization time constant and t is the time from the onset of ionization.

As the current decreases the resistivity shall recover to its original value $\rho_o$ in a time dependent exponential manner but also current density dependent. The transition from the lower state back to the $\rho_o$ value is given by:

$$( 1 - \exp( - t / \tau_2 ) ) ( 1 - J/J_C )^2 \qquad \text{(Eq 5)}$$

Where $\tau_2$ is the deionization time constant, and $t$ is the time measured from the instant of decay. J is the current density in the soil and Jc is the critical current density of the soil. The second term is included on an energy consideration - the longer the tail of the current wave, or the more energy injected into the soil, the longer the resistivity will remain low.

The critical current density relation to the critical electric field is given by:

$$Ec = Jc * \rho_o \qquad \text{(Eq 6)}$$

The resistance of a single driven rod is given by [7] :

$$R_E (\text{rod}) = \rho / 2\pi l \times \ln ((r_o + l) / r_o) \qquad \text{(Eq 7)}$$

Fig 1.1 Simplified model for resistance of a single driven rod

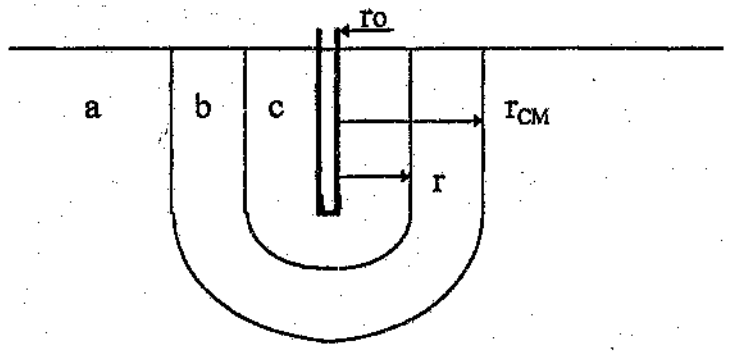


* r is the apparent radius of the electrode.
* $r_{CM}$ is the maximum apparent radius of the electrode corresponding to the peak current value.

During impulse conditions in a single driven rod - three regions in the soil are considered:

i) Region a - where $r > r_{CM}$ and $J > Jc$ in this region $\rho = \rho_o$
no ionization takes place.

ii) Region b - where $r < r_{CM}$ and $J < Jc$

The current density J is below the critical value and the soil resistivity recovers in the following manner:

$$\rho = \rho_i + (\rho_o - \rho)(1 - \exp(-t/\tau_2))(1 - J/J_C)^2 \qquad \text{(Eq 8)}$$

where $\rho_i$ is the soil resistivity value when $J = J_C$

iii) Region c - where $r < r_{CM}$ and $J > Jc$

The current density J exceeds the critical value and ionization takes place:

$$\rho = \rho_o \exp(-t/\tau_1) \qquad \text{(Eq 9)}$$

This will persist until the point $J = J_C$ when it enters region b.

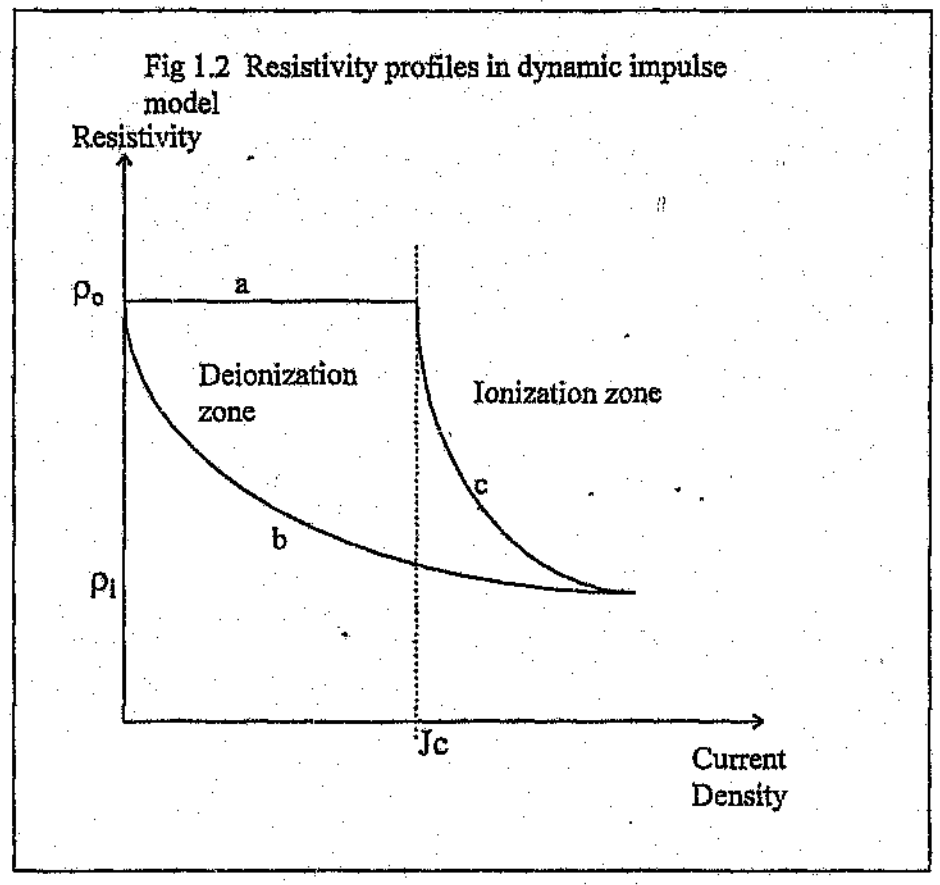


Fig 1.2 Resistivity profiles in dynamic impulse model

The current impulse and the nonlinear resistance can be represented by an equivalent circuit shown in figure 1.3 below. The solution of this circuit is based on a time-iterative energy balance method which has been executed on a digital computer. The results compared very well with experimental values [7].

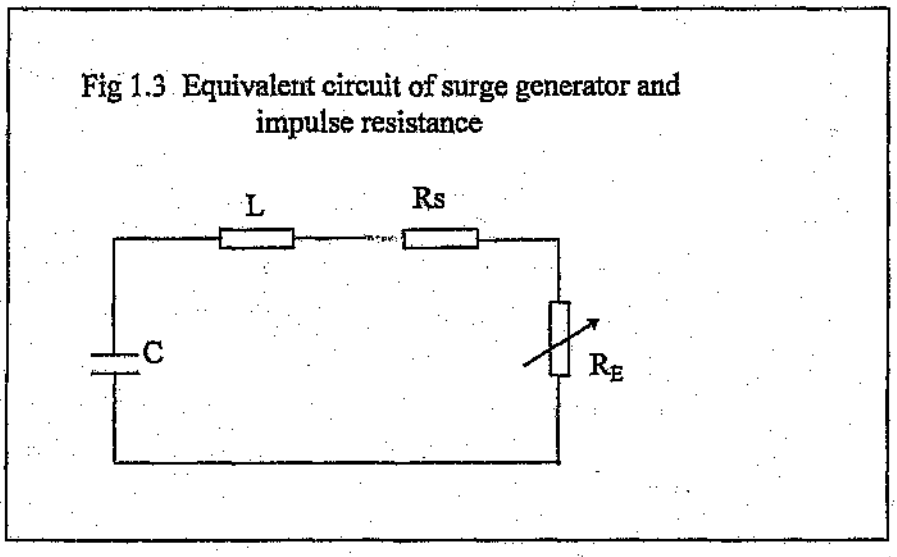


Fig 1.3 Equivalent circuit of surge generator and impulse resistance

A similar model has been implemented recently on **EMTP** [13] with very good agreement between computed results and measured results.

**Similarity approach - Korsuncev , Chisholm**

A second model was originated by Korsuncev and extended by Chisholm .
In 1958 Korsuncev applied similarity analysis to the surge respone of ionized soil around earth electrodes. He concluded that footing resistances of differing ground electrodes geometries can be represented by two dimensionless parameters $\Pi_1$ and $\Pi_2$ :

$$\Pi_1 = sR_E / \rho \qquad \text{(Eq 10)}$$

$$\Pi_2 = \rho I / E_c s^2 \qquad \text{(Eq 11)}$$

s is the characteristic distance from the center of the electrode to the outermost point .
$\rho$ is the oil resistivity.
$R_E$ is the electrode resistance.
I is the electrode current.
$E_c$ is the critical breakdown field.

For each electrode geometry a value of $\Pi_1^0$ is defined in terms of its low frequency low current resistance. $\Pi_1^0$ values for typical electrode configurations lie within the range of 0.2 to 0.8, with hemisphere like electrodes having the lowest values and single rods having the highest values. $\Pi_1^0$ values can also be approximated in terms of the distance s and the electrode surface area A [12].
For example for a single rod and a hemisphere the following values of $\Pi_1^0$ result:

$$\Pi_1^0(\text{rod}) = 0.4028 + (1/2\pi) \times (\ln s^2/A) \qquad \text{(Eq 12)}$$

$$\Pi_1^0(\text{hemisphere}) = 0.4517 + (1/2\pi) \times (\ln s^2/A) \qquad \text{(Eq 13)}$$

For Geometry dependent region ($\Pi_1$ = constant) - The characteristic distance s and the surface area A are computed and equation (13) gives the $\Pi_1^0$ value. Equation (10) is then used to compute the electrode resistance $R_E$.

For Geometry independent region ($\Pi_1 = f(\Pi_2)$) - Once ionized beyond the critical distance, all electrodes behave much like a hemisphere. Korsuncev has developed a critical curve $\Pi_1 = f(\Pi_2)$, a least-squares fit to this curve in the range of 0.3 to 10 gives the following power-law relation:

$$\Pi_1 = 0.2631\Pi_2^{-0.3082} \qquad \text{(Eq 14)}$$

The power-law relation between the soil resistivity and the critical field is given by [12]:

$$E_C = 241\rho^{0.215} \qquad \text{(Eq 15)}$$

The transition between low current and ionized respone occurs when $\Pi_1$ value from equation (14) becomes smaller than $\Pi_1^0$.

The combination of the two regions gives a complete model:
For low currents an initial resistance is calculated from equations (13) and (10). For higher currents equations (11) and (15) provide $\Pi_2$ value and the $\Pi_1$ value is calculated from equation (14). As long as the $\Pi_1$ value is lower than the $\Pi_1^0$ value the ionization has spread beyond the characteristic distance and the surge reduced resistance is calculated from equation (10).

Comparison with results from the Liew and Darveniza model show that the initial low current resistances are lower in the Chisholm model and the surge reduced values fall more quickly with applied current. Both models converge to the same impulse resistance at high currents.

**Experimental work in South Africa**

Experimental work on practical earth electrodes, which included impulse tests of a ring and a single rod, was done by Oettle and Geldenhuys [11]. The current flow into ohmicaly separated sections of the electrodes was monitored.
It was concluded by the authors that the model of a uniform ionization zone which is said to surround the electrode whenever the critical electrical field is exceeded was not representative of the physical processes involved under high voltage impulse conditions.
However it was acknowledged that the mathematical model describing the phenomena would be extremely cumbersome and not practical for engineering situations.
The authors suggested that the uniform ionization zone model could be used as an empirical means of comparing the impulse impedance and the critical electrical field of various electrodes in different soil conditions.

### 1.2.4 Extended electrodes - Dynamic models

Extended electrodes are beyond the scope of this project. However, for completeness a short description of their behaviour modelling is given:

Two similar models have been proposed by Mazzetti and Veca [8] and Velazquez and Mukhedkar [9] -
A single horizontal buried conductor is modelled by a distributed parameter representation of the leakage conductance G, inductance L, capacitance C and resistance R - all per unit length as illustrated in Figure 1.4 below:

Fig 1.4 Representation of ground electrode with uniformly distributed parameters

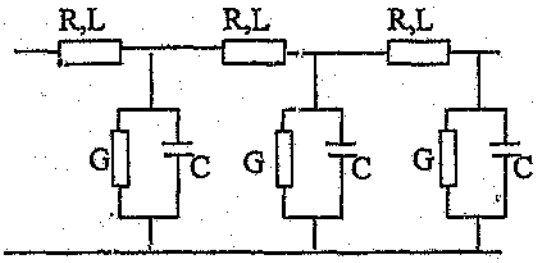

This representation is similar to a long transmission line. The only difference is that the resistance is negligible compared to the inductance, and the capacitance is negligible compared with the conductance.

The propagation of surge impulse currents into the soil can be considered to be governed by laws typical to a conductive medium [8] [9]. Therefore, the wellknown equations of propagation may be integrated in order to obtain the behaviour of the voltage and current along the electrode, as well as the impulse impedance.

The soil breakdown that occurs when a high impulse current is injected into the electrode has been considered in the model as an apparent increase in the cross-section of the electrode and therefore a decrease in ground resistance.

## 2. POWER FREQUENCY

### 2.1. Experimental Set-up and Testing Procedure

#### 2.1.1. Step potentials - field measurements

The tests were performed at the outdoor high voltage laboratory of the SABS National Electrical Test Facility (NETFA), Olifantsfontein. An HV Lab and test site plan is shown in Fig 2.1. Five different electrodes were installed at four locations in the open field adjacent to the HV Lab concrete floor. The distance between the nearest electrode (A&B) and the concrete floor was about 80m.
A single phase 1.2MVA multi-tap transformer was used as an AC source. A single phase 22kV line was built to supply the installed electrodes. This line was latter used for impulse test measurements.

Fig. 2.1 HV Lab and test site plan

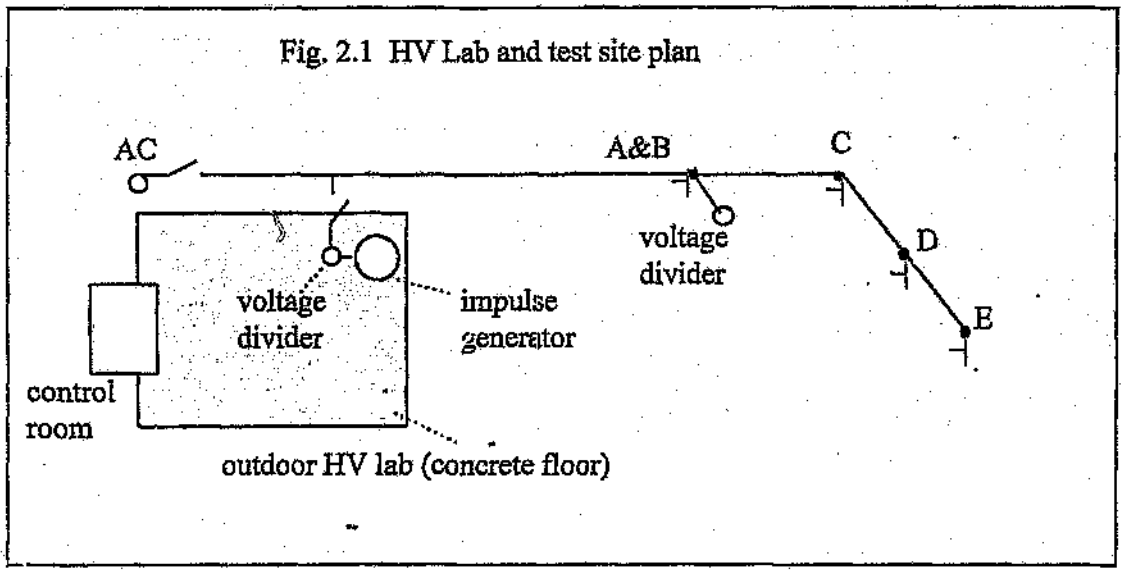


A detailed soil resistivity survey of the field where the electrodes were installed was performed -results are shown in Appendix D. The various electrode configurations which were tested for step and touch potentials are illustrated in Fig 2.2. The dimensions are given in Table 2.1.

Table 2.1 Electrodes dimensions

| Dimensions | A | B | C | D | E |
|---|---|---|---|---|---|
| trench length (m) | 6 | 6 | 10 | 8 | 6 |
| depth (m) | 1 | 1 | 1 | 1 | 1 |
| rod length (m) | 1.5 | 3 | 1.5 | 1.5 | 1.5 |
| no of rods | 4 | 4 | 1 | 7 | 4 |

Fig. 2.2 Test set-up : Step potential and electrode resistance measurement

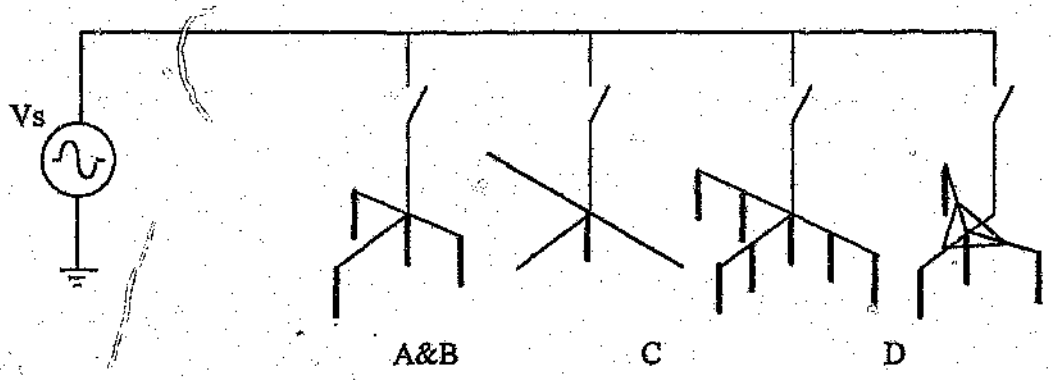


* The star point of the electrodes was located 1m away from the pole.

**Test procedure**

Each electrode was connected to the supply line, one at a time, using an earth lead which ran up the associated wooden pole. The output voltage of the supply transformer was chosen as 250V because of earth fault protection considerations. Once the line was energised, the voltage on the surface of the earth was measured using the following method:

A reference spike was driven into the ground at a distance of about 25m from the point were the earth down lead entered the ground - at right angles to the supply line. Then a multimeter was used to measure the voltages between the various points on the surface of the earth around the electrode ( at intervals of 1m)

Fig 2.3. Step potential -method of measurement

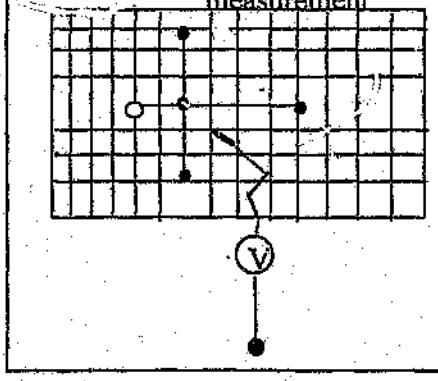

The voltage of the earth down lead and the current at the point of entry to the ground were also measured in order to calculate the apparent low frequency resistance of the electrode. In a separate test the resistance of the electrodes were measured using an earth resistance megger.

Observation:
It was observed that after a period of time (about 40min) the current would start to drop significantly, e.g. 42A to 32A.
Thus if the current started to drop during the measurements, the test was then stopped for a while and resumed later at the previous current level.
This phenomena is attributed to the heat which is generated in the vicinity of the buried conductors ($I^2R$ losses). The heat dries the soil and thus the electrode resistance increases which results in a lower current.

### 2.1.2 Electrolytic Tank-Step Potential

**The measuring circuit**

The tests were performed at the Wits HV laboratory. Scale models of the various electrodes were submerged in water inside an electrolytic tank. The tank diameter was 3m and the height was 1.2m.
The tank was first lined with aluminium foil on the sides and the bottom and then filled with water to a level of 1m. The scale electrode was constructed using Nichrome wire of 0.173mm diameter (scaling factor of 57.8). Nichrome wire was selected because it is mechanically more rigid and tends to oxidise less than copper.
The electrode was supported by a perspex structure and nylon strings.

A 230/24V transformer was used as a source in series with a variable resistor. An illustration of the circuit is shown in Fig 2.4 below.

Fig. 2.4 Electrolytic tank test set-up

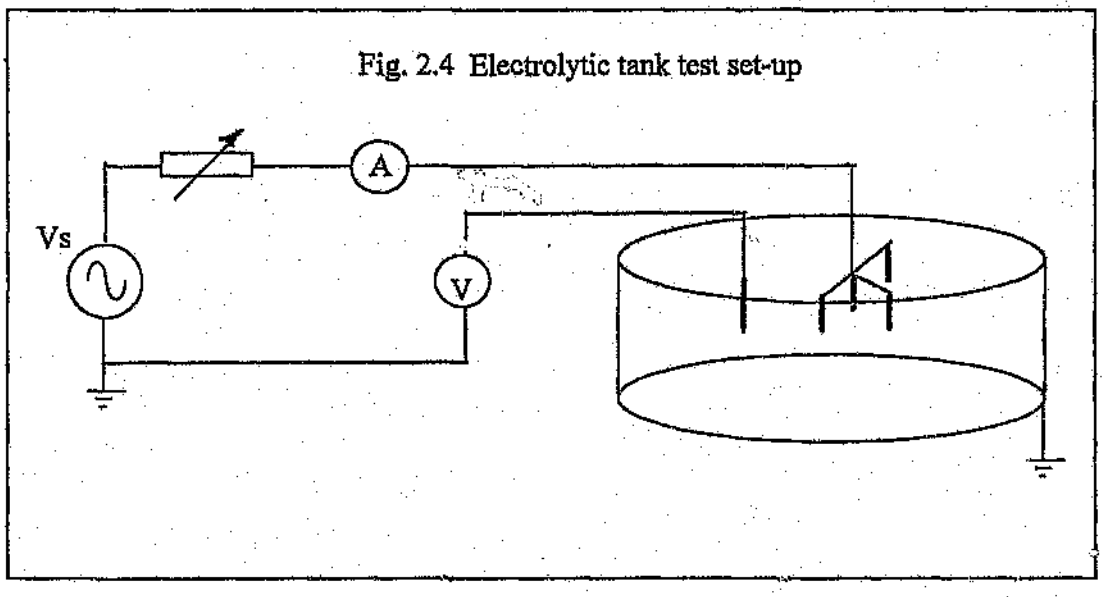

**Test procedure**

The surface potentials around the electrode under test were measured using the following method:

A square 3mx3m wood frame was fitted on top of the tank edge and measuring tapes were attached to the top side of the wood on two parallel sides - which was the Y-axis. A 3m wood beam fitted with a plastic curtain rail and measuring tape was laid on top of the wood frame and a voltage probe was attached to a slider which was free to move along the curtain rail - which is the x-axis.

The voltage probe was adjusted in such a manner so that its tip was 1cm below the water surface. Fig 2.5 shows a top view of the measurement accessories.

Fig 2.5. Measurement method

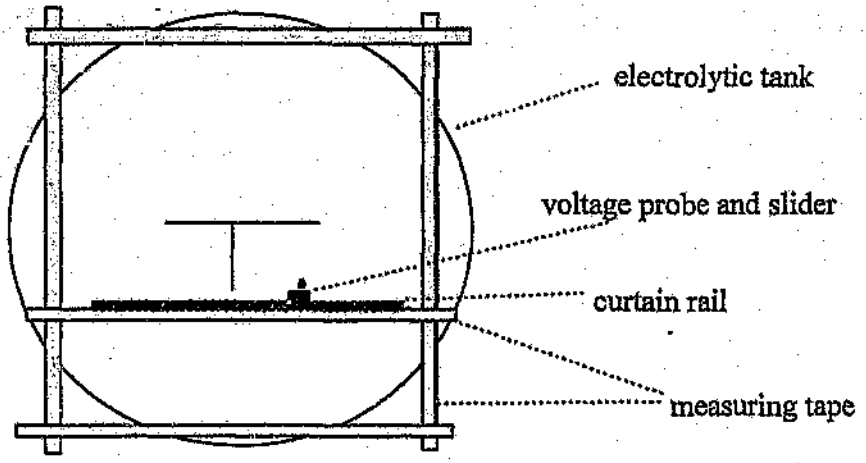


Measurements were taken at intervals of 2cm.

## 2.2 Presentation of results

### 2.2.1 Field measurements

The results of surface voltage measurements of all the electrodes are presented in Appendix A in the form of equipotential lines.

The surface equipotential voltages of electrode B are plotted in Fig 2.6 on the next page.

Fig 2.6 Surface equipotentials for electrode B

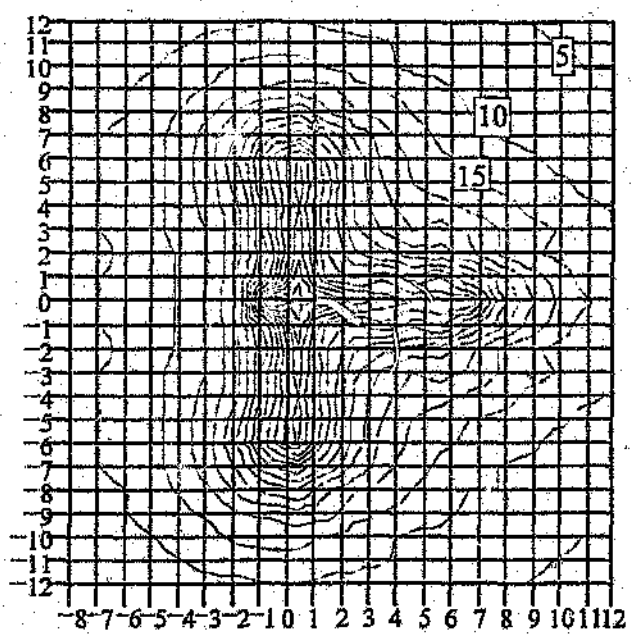


Contours

minimum value 5V
maximum value 80V
steps of 5V

B1

**Electrode resistances**

The apparent low frequency resistance of the test electrodes is shown in table 2.2 below

Table 2.2 : Apparent low frequency resistance of test electrodes

| Electrode | Voltage (V) | Current (A) | R= V/ I (Ω) | R megger (Ω) |
|---|---|---|---|---|
| A | 233 | 10.1 | 23.07 | 31.3 |
| B | 203 | 41.8 | 4.85 | - |
| C | 230.8 | 5.8 | 39.8 | 34 |
| D | 226.5 | 9.5 | 23.8 | 23.1 |
| E | 227 | 6.2 | 36.6 | 26.4 |

### 2.2.2 Electrolytic tank

The results of the surface potentials of electrodes F and G are included in Appendix B.

The surface equipotentials of electrode F are plotted in Fig 2.7 below

Fig 2.7 Surface Equipotentials for electrode F

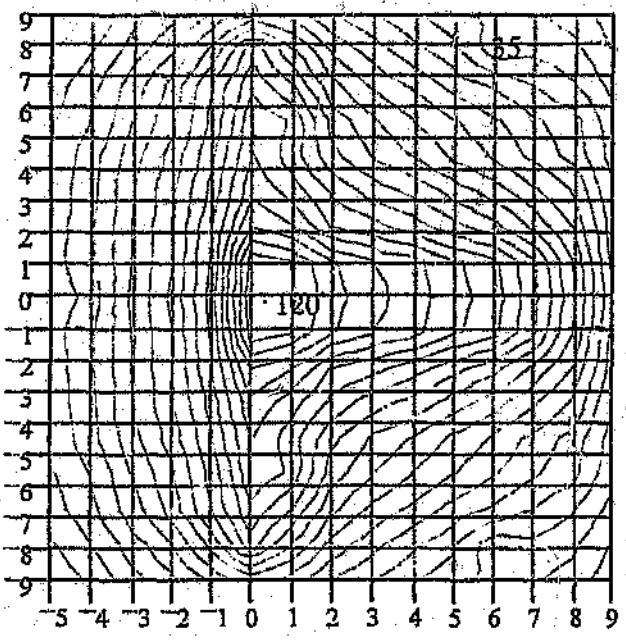


F1

Contours
(Scaled up)
minimum value 25V
maximum value 125V
steps 7.5V

Grid lines:
1m x 1m
(Scaled up)

### 2.3 Interpretation of results

**Soil resistivity**

Examination of the soil resistivity survey results suggests two features

a. The soil resistivity at each location decreases with depth. The resistivity at a depth of 10m is 10 to 15% of the resistivity at the top layer.
b. The soil resistivities at the various locations at the test field are all in the same order of magnitude of a few hundred Ohm at the top layer.

**Electrode resistances**

Examination of the different electrode resistances (table 2.2) indicates the following:

a. There was a significant reduction in resistance when electrode A was changed to electrode B (using 3m rods instead of 1.5m).
   This is attributed to the fact that the soil resistivity decreases with depth.
b. The electrode C resistance was the highest although it had the longest trench (10m). This could be attributed to the fact that it has got only one rod
c. The electrode D resistance was almost equal to the electrode A resistance although it had a longer trench (8m) and 3 extra rods.
   This could be attributed to the fact that the soil resistivity around the electrode D location are higher than that around electrode A.
d. The electrode E resistance was higher than D although the total trench length of both was the same (about 24m). This could be attributed to the fact that Electrode E has less rods (4) than electrode D (7) and the soil resistivity was slightly higher around E.

**Scaling up of field measurements**

The step potential tests were performed using a supply voltage of 250V. However, operating voltages on MV networks are 11kV and 22kV with 6.35kV and 12.7kV line to ground voltages respectively.

Therefore the following scaling factors can be calculated:

$$SF_{11} = \frac{6350}{250} = 25.4$$

$$SF_{22} = \frac{12700}{250} = 50.8$$

Scaling of the electrolytic tank measurement was done as follows:

1. The actual electrode voltage, measured at the field, was divided by the respective electrode voltage, measured at the tank.
2. The tank electrode resistance was divided by the field electrode resistance.
3. The earth soil resistivity at 2m depth was divided by the water resistivity (50Ωm).

The scaling factor was taken as: (1)x (3)/ (2)

The comparison of the results for two electrode configurations gives an error of 15% to 40% which is not acceptable. This shortcoming is probably because of the fixed electrolytic (water) resistance in comparison to the soil resistivity in the field , which dropped rapidly with depth.

## 2.4 Discussion

From the results for the electrode resistances it is clear that the addition of rods with the same length to the configuration does not reduce the resistance significantly. However, extension of existing rods where the resistivity of the soil decreases quickly with depth, results in dramatic decrease in the electrode resistance. This would probably not be true for soils with constant resistivity, or where the resistivity increases with depth.

For electrode configurations which are more "symmetrical" (e.g. electrode E is more symmetrical than electrode A ) - the maximum step potentials are lower. However, the improvement is not significant. It is probably better to put effort into reducing the electrode resistance in order to reduce the maximum electrode voltage during a fault. A reduction in electrode voltage will inherently reduce the step potentials around it.

Fig 2.8 below shows the electrode voltage and current as a function of its resistance. The values where calculated for a 22kV system with a fault level of 14kA and a Neutral Electromagnetic Coupler, which limits the fault current to 300A. Two different line lengths from the source substation to the fault location, were taken into account 1km and 10km.

There is a change in the voltage slope around the value of 40Ω, below which the electrode voltage drops rapidly when the resistance is decreased.

Fig 2.8 Earth electrode current and voltage vs electrode resistance

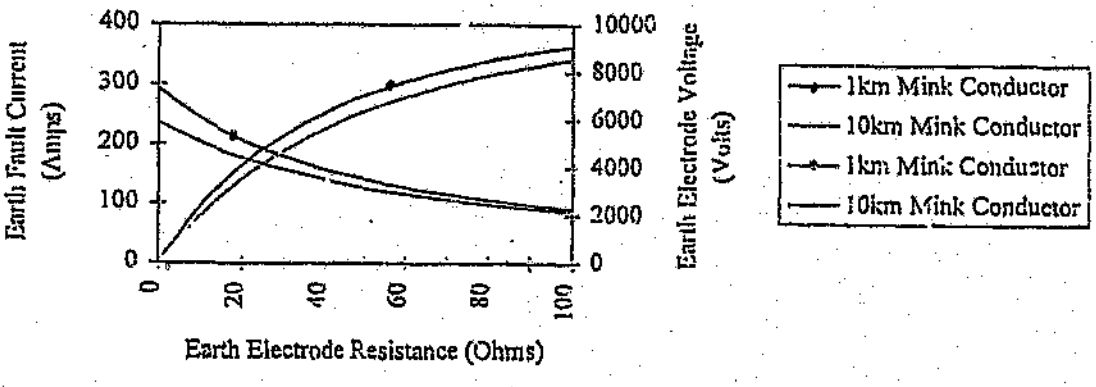

# 3 IMPULSE BEHAVIOUR

## 3.1 Experimental set-up and testing procedure

### The measuring circuit

The tests were performed at the outdoor HV laboratory of NETFA. The test site plan is shown in Fig 1.1. Tests were carried out only on electrodes A and B at the same location (see dimensions of table). Fig 3.1 illustrates the electrical test circuit. Fifteen of the impulse generator capacitors were utilised and connected in series.

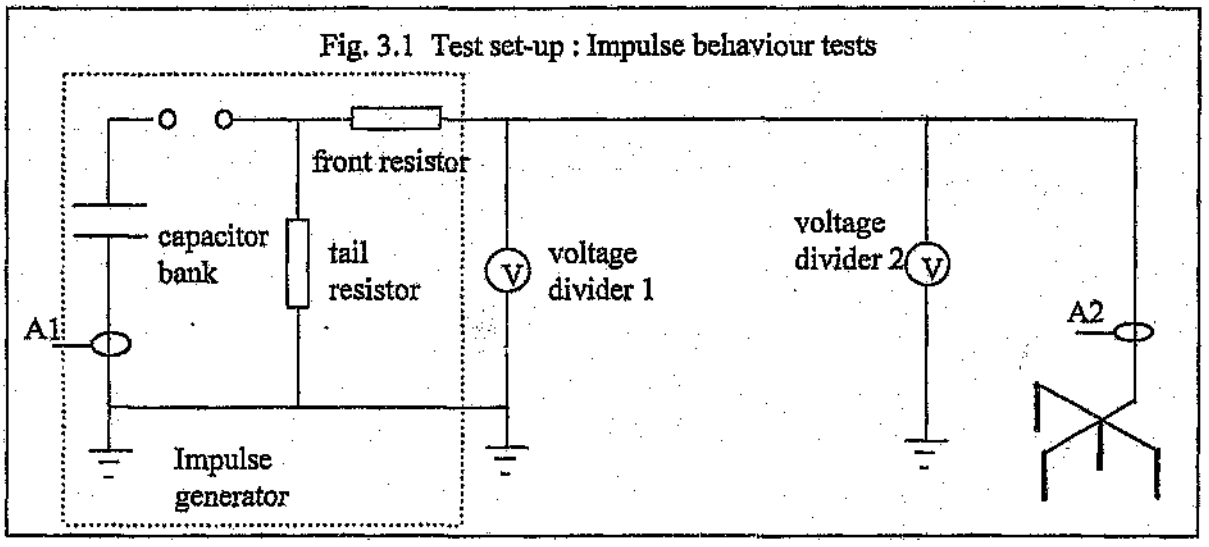


Fig. 3.1 Test set-up : Impulse behaviour tests

Two voltage dividers were used:
- voltage divider 1: at the output of the impulse generator, using the HV laboratory earth mat as a reference.
- voltage divider 2: at the electrode under test - the reference was achieved by driving spikes at a distance of 25m away from the point where the electrode down lead enters the ground - at right angles to the supply line. These spikes were then connected to the LV side of the voltage divider by means of a Mink conductor (11mm diameter).

A current transformer (Pearson coil A1) was used to measure the generator output current. A second current transformer (Pearson coil A2) was placed at the point of entry of the earth down lead into the ground to measure the input current into the earth electrode under test.

In order to measure the current distribution in the ground electrode seven wide band current transformers were installed. These wide band current transformers were of the Rogowski coil type. The location of each coil is shown in figure 3.2.

Fig. 3.2 Location of Rogowski coils for current distribution measurement

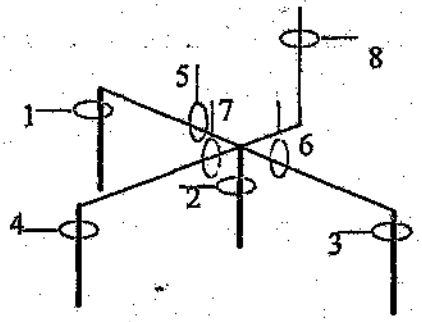


Coils 1,2,3,4 were installed around the rods, just below the connection between the rod and the conductor in the trench. Coils 5,6,7 were installed around the conductors in the trench about 40cm from the star point. Coil 8 was installed around the earth down lead.

Coaxial cable leads were taken up vertically from the Rogowski coils to where they were connected to optical transducers. From there optical fibre cables were taken to the HV measurement truck which was positioned 50m away. The physical distance between the generator output and the electrodes along the connecting line was 110m.

The voltage and current at the generator output were recorded on a Tektronics Scope using separate channels. The electrode voltage and currents were recorded at the HV measurement truck using the Nicollet facility which is a computer based data acquisition system for high voltage transient measurements.

**Test procedure**

Electrode A was subjected to a series of impulses starting from a 30kV generator charging voltage up to 150kV. Voltage and currents were recorded at the points mentioned in the previous section.

Once the electrode A tests were completed the 1.5m rods were pulled out and 3m rods were installed instead - this new configuration was named electrode B.

## 3.2 Presentation of results

### 3.2.1 Impulse waveforms

Typical voltage and current waveforms which were recorded are shown below.

Fig 3.3 : Generator output waveforms

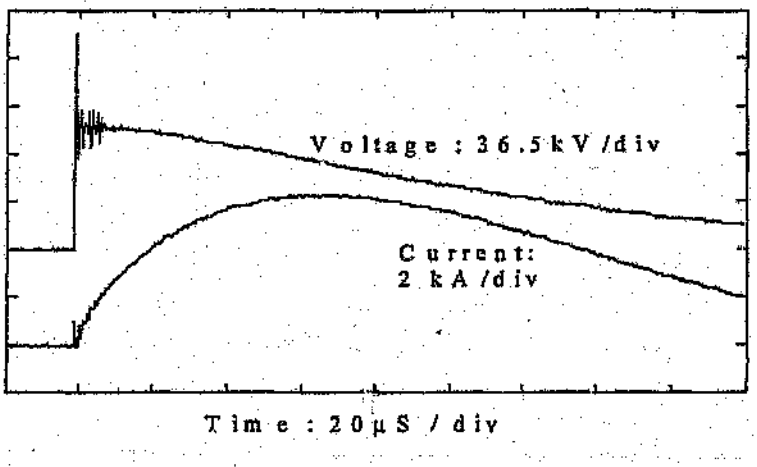


Fig 3.4 : Voltage and total current at the electrode

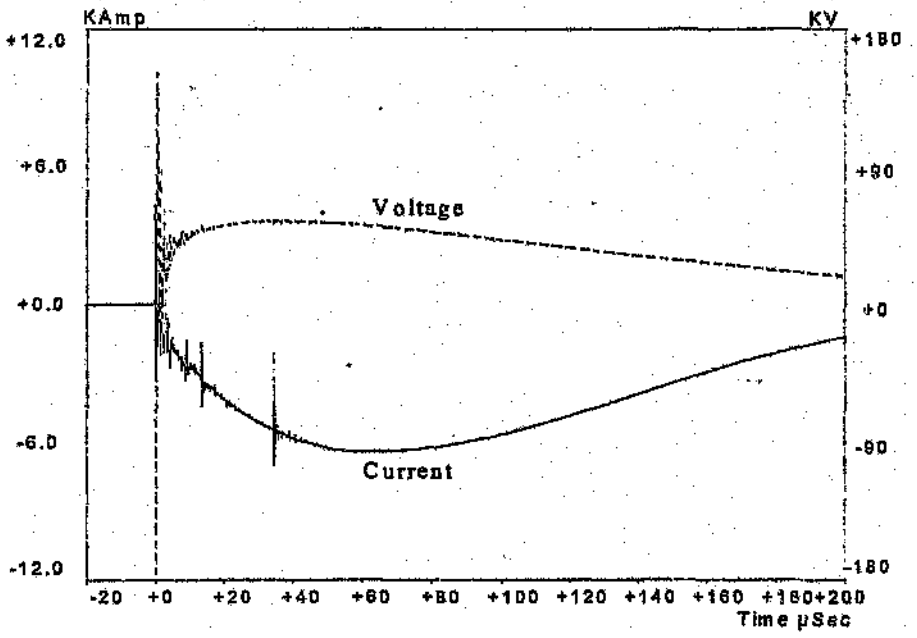

Fig 3.5: Impulse currents in coils #4 and #7

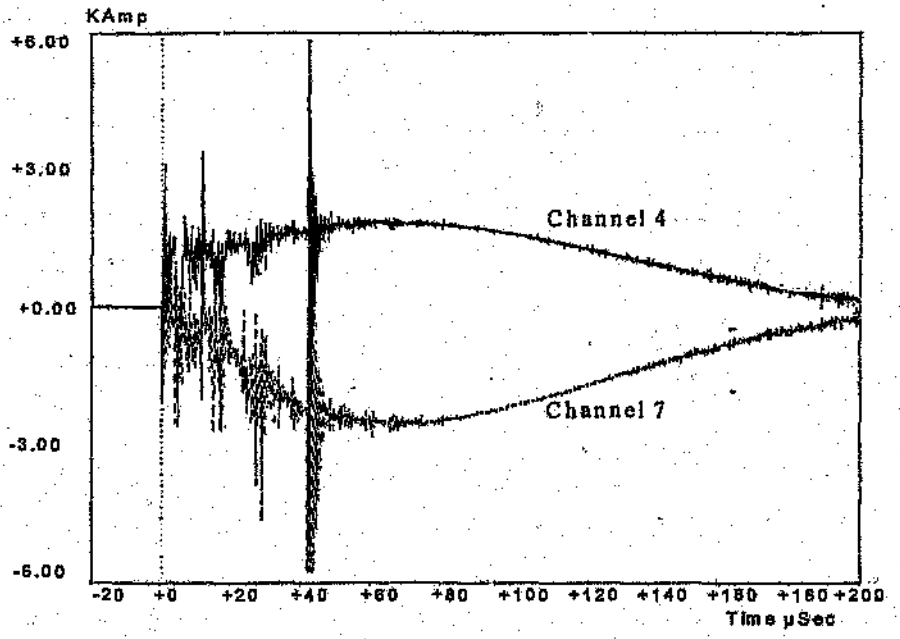


The waveforms above were imported directly from the measurement instruments. Test waveforms for the various voltage levels can be found in Appendix E.

### 3.2.2 Current distribution

The distribution of currents in the electrode were calculated using the peak current values of the waveforms on the legs of the three point star electrode (coil #4 and coil #7) as well as the rod which was installed at the star point (coil #2).

The current in coil #7 was chosen as reference (100%). Then the current in the other coils was measured and calculated as a percentage of the current in coil #7.
There was some diversity in the results. The same exercise was done using power frequency. Fig 3.5 below shows the distribution of currents under low frequency conditions.
A summary of the results of electrode A is given in Table 3.1 below.

Table 3.1 : Distribution of current in the earth electrode

| Type of Test ↓ | Coil Current #7 | Coil #4 Current relative to #7 | Coil #2 Current relative to #7 |
|---|---|---|---|
| AC | 100% | 27%-33% | 22%-33% |
| Impulse | 100% | 75%-90% | 95%-130% |

Fig 3.6 Distribution of power frequency current electrode A

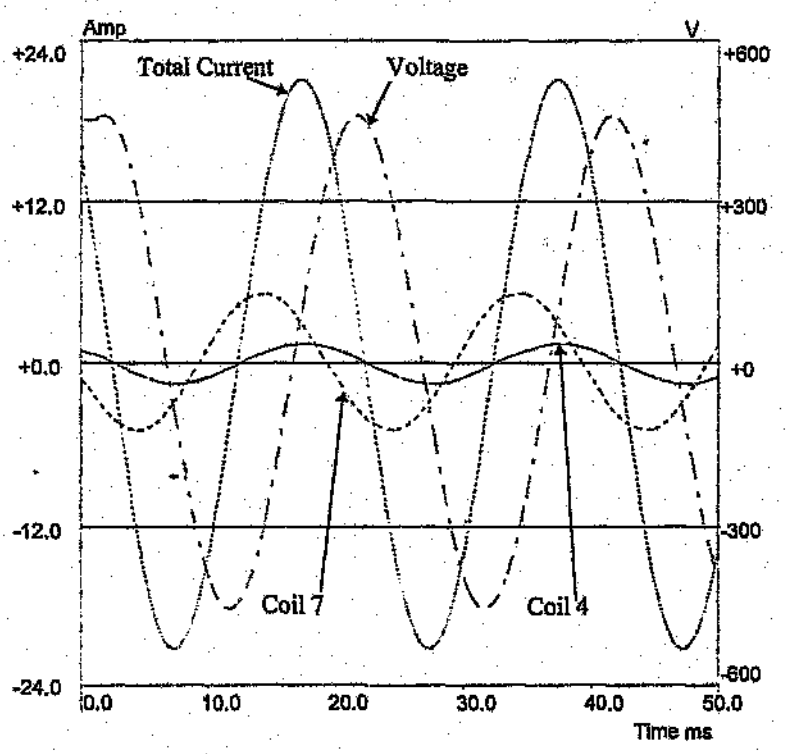

## 3.3 Interpretation of results

### 3.3.1 Reduction in electrode resistance

Fig 3.7 Electrode Resistance vs Peak Current

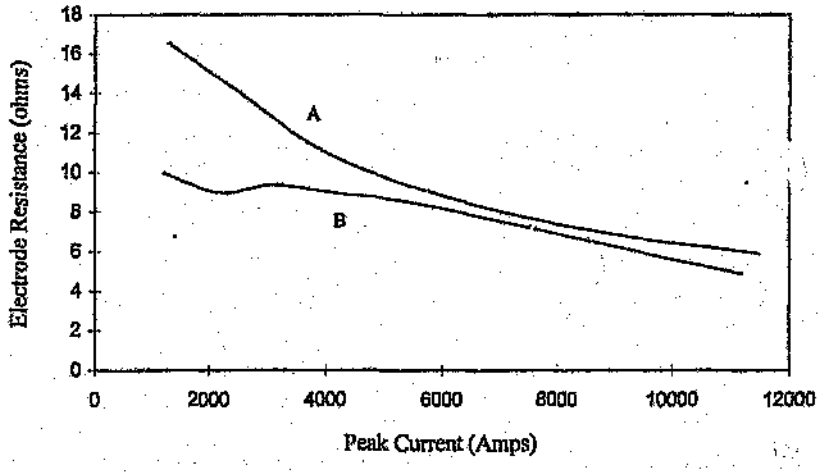


Figure 3.7 above demonstrates the reduction in the conventional electrode impedance. the curve for electrode A gives a reduction factor (from its power frequency low current value) of 3 to 3.5 at currents with a peak greater than 8kA. However the electrode B reduction factor is only unity. This could be attributed to drying of the soil around the electrode during tests. It was also noticed during step potential measurements on this electrode configuration that the apparent resistance was increasing with time and the test had to be stopped for a while.

The slope of the curve for electrode A is much steeper than that for electrode B - this agrees with previous studies where it was normally found that where the low frequency low current
impedance is high the fall to a reduced value is faster [7] [12].

From Figures 3.3 and 3.4 it is noted that the front of the voltage wave form as measured at the output of the generator is much steeper than at the electrode - This is the effect of the long loop inductance. The peak voltage drop (20% to 25%) is also attributed to the long distance that that surge has to travel.
The current peak at the electrode occurs after the voltage peak. There is a time delay of about 50 mS.
Both currents, which were measured with separate and different instruments, at the electrode and at the generator have the same peak magnitude. Therefore the results could be taken as correct with relatively high confidence.

### 3.3.2 Current Distribution

The difference between the #7 and #4 currents is the current which dissipates from the conductor in the trench. The lengths and current distribution at low frequency is given in table 3.2 below. It appears that the currents dissipating from the conductor in the trench and from the rod are proportional to their length.

Table 3.2 Power frequency current - proportional distribution

| | length (m) | dissipated current (%) |
|---|---|---|
| conductor in trench | 5.5 (80%) | 70% |
| rod | 1.3 (20%) | 30% |
| total | 6.8 (100%) | 100% |

However under impulse conditions most of the current (75-90%) is being dissipated from the rods. Furthermore, rod #2 is dissipating more current than rod #4. This could be attributed to the fact that rod #2 is closer to the point of current injection.

In Fig 3.6 there are phase shifts between the various currents, while one would expect to have them all in phase because the electrode is treated as a resistance. These phase shifts could be attributed to the integrators in the Rogowski coils.

### 3.4 Discussion

In general the results which were obtained from the impulse tests agree with previous published work [7] [11][12] - there is a reduction of electrode impedance under impulse conditions. The current peak occurs after the voltage peak - this can be attributed to the ionization time constant [7] [10] [11].

The more interesting observation from this work is the different current distribution between the electrode components under impulse conditions. It appears that heavy ionization is taking place around the rods rather than around the trench conductors. The soil resistivity around the rods is lower by a factor of 2 to 3 compared with around the trench conductors. Lower soil resistivity implies that for ionization to take place a higher current density is needed. The nonuniform electric field near the tip of the rods may also contribute slightly to the increased ionization.

# 4 CONCLUSIONS AND RECOMMENDATIONS

## 4.1 Conclusions

1. Where soil resistivity decreases with depth, use of extended rods in the electrode configuration results in significant decreases in electrode resistance.

2. Changing the configuration of an electrode to a more symmetrical shape does have an effect on the maximum step potential. However this effect is not significant.

3. Results of scale model tests in an electrolytic tank did not agree well with the field measurements. It is concluded that the problem is that the water in the tank is homogenous, whereas the soil resistivity in the field decreased rapidly with depth.

4. Reduction factors (from the initial low frequency low current electrode impedance to the value under impulse conditions) of 3 to 3.5 were recorded.

5. The current distribution between the electrode components is different for power frequency and for impulse conditions. For power frequency conditions the distribution of currents is proportional to the length of the conductor or rod. However for impulse conditions most of the current is dissipated from the rods due to higher ionization. This statement is true for soils with decreasing resistivity with depth.

## 4.2 Recommendations for further work

**Power frequency**

It is recommended that a computer modelling be used to try to reconstruct the results obtained from the full scale model. Such a simulation could then be used to optimise electrode configuration design

**Impulse behaviour**

Impulse tests on electrodes buried in a soil with constant resistivity and tests on electrodes with no rods at all would probably provide a more complete understanding of their behaviour.

## APPENDIX A - FIELD MEASUREMENTS RESULTS

Fig A1 : surface equipotentials for electrode A

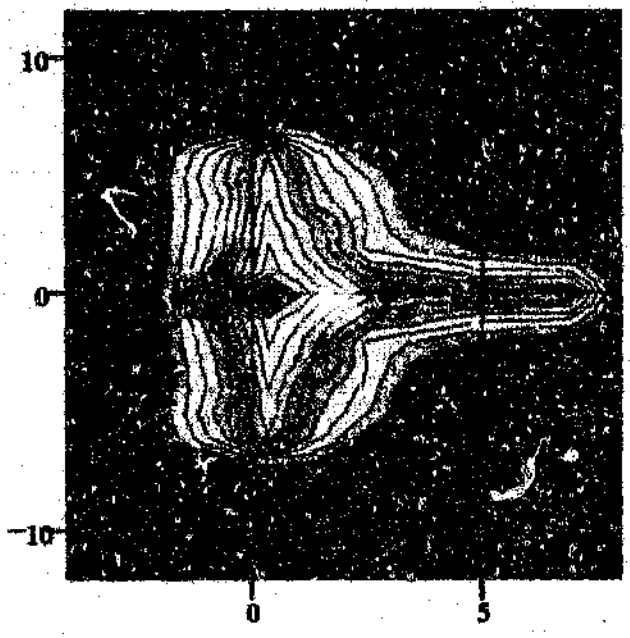


A1

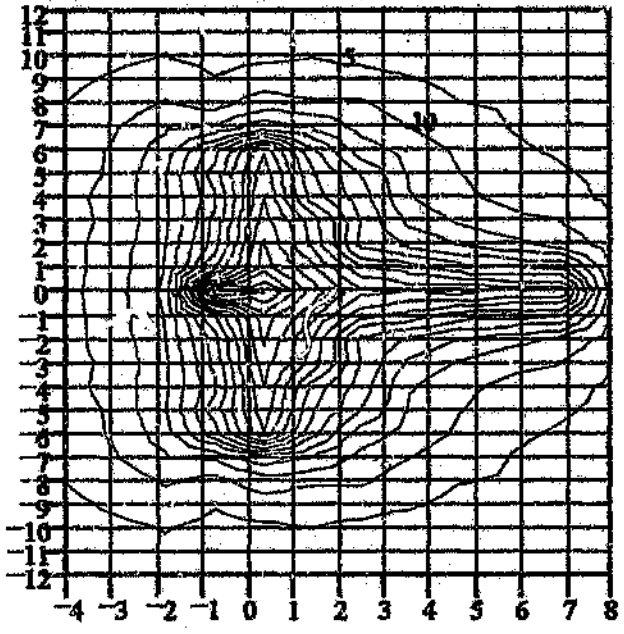


A1

configuration:

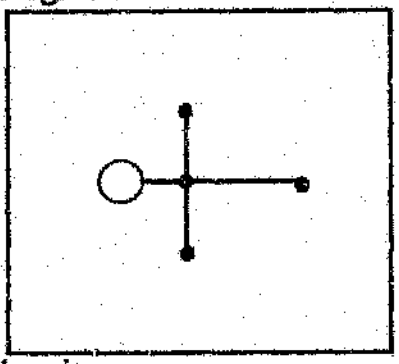

Dimensions:

| | |
|---|---|
| trench depth | 1m |
| radial length | 6m |
| rod length | 1.5m |
| number or rods | 4 |

* V = 233V
* I = 10.1A
∴R = 23.0Ω
* measured at the point where the earth lead enters the ground

** Rmegger = 31.3Ω
** measured using an earth resistance megger (DET5)

Contours

minimum value 5V
maximum value 70V
steps of 5V

grids

1m x 1m

Fig B1 : surface equipotentials for electrode B

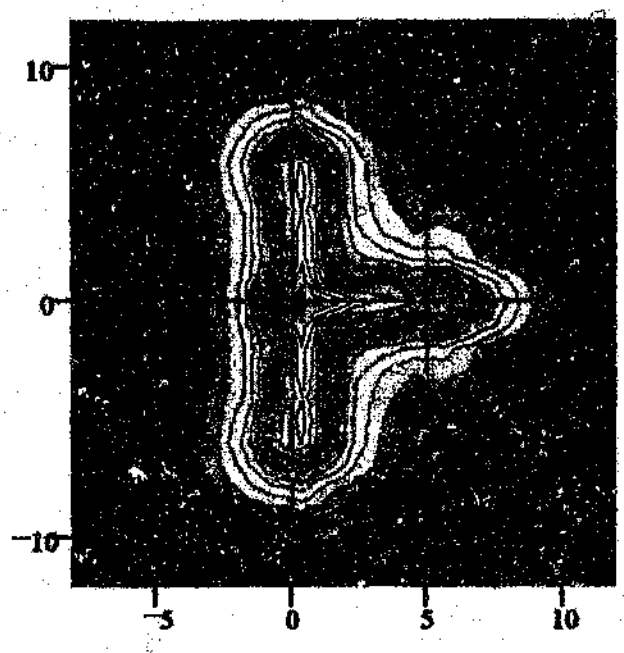


B1

Cofiguration:

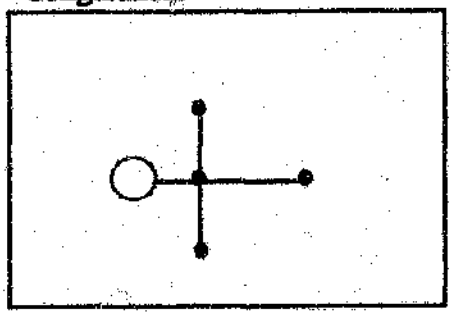

dimensions

| | |
|---|---|
| trench depth | 1m |
| radial length | 6m |
| rod length | 3m |
| number or rods | 4 |

* V = 203V
* I = 41.8A
∴R = 4.85Ω
* measured at the point where the earth lead enters the ground

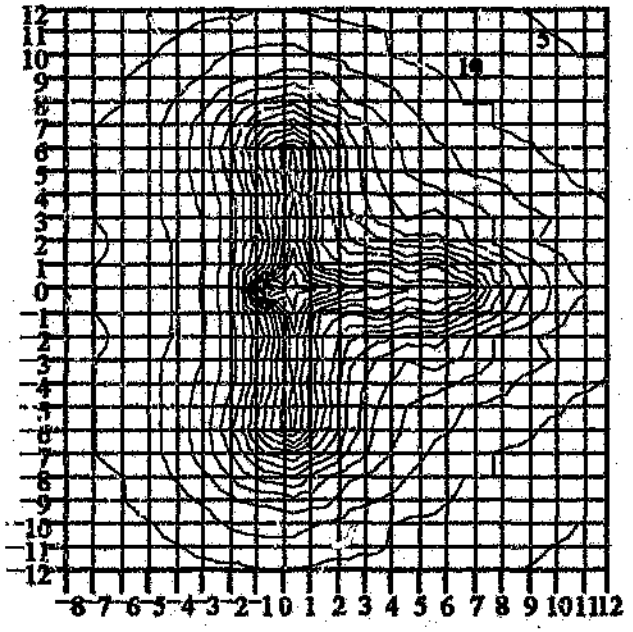


B1

Contours

minimum value 5V
maximum value 80V
steps of 5V

grids

1m x 1m

Fig C1 : surface equipotentials for electrode C

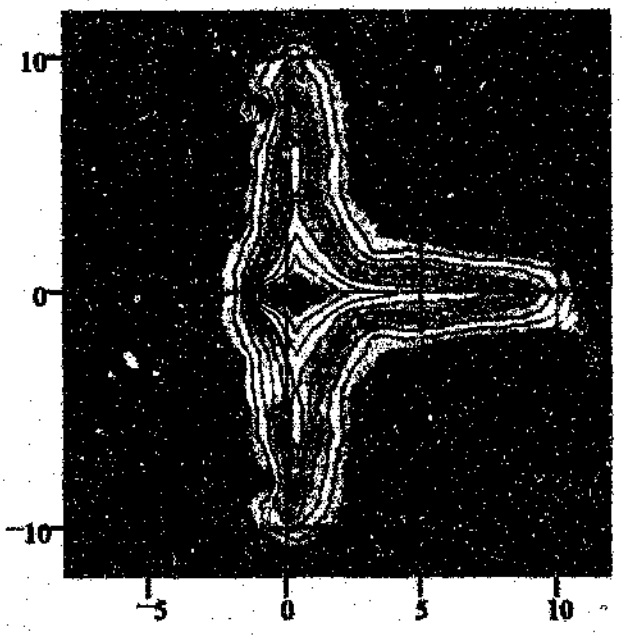


C1

Configuration:

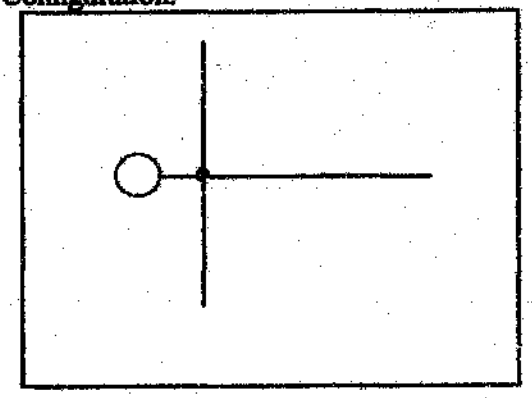

Dimensions

| | |
|---|---|
| trench depth | 1m |
| radial length | 10m |
| rod length | 1.5m |
| number or rods | 1 |

* V = 230.8V
* I = 5.8A
∴R = 39.8Ω
* measured at the point where the earth lead enters the ground

** Rmegger = 34Ω
** measured using an earth resistance megger (DET5)

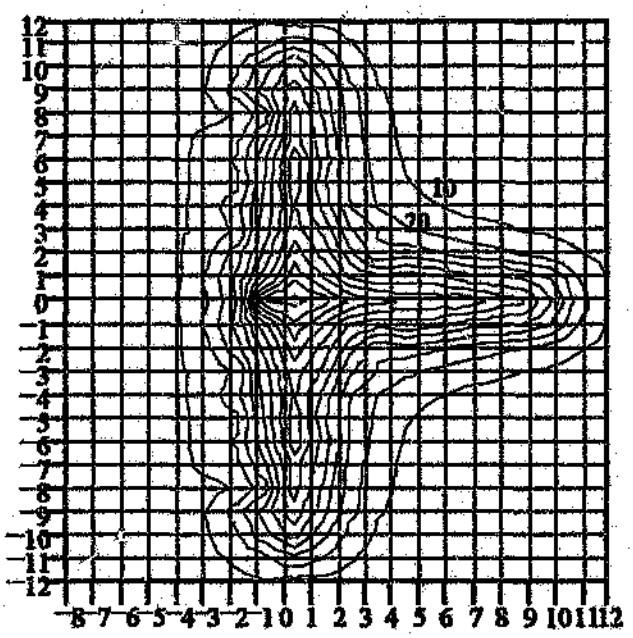


C1

Contours

minimum value 10V
maximum value 100V
steps of 10V

grids

1m x 1m

## Fig D1 : Surface equipotentials for electrode D

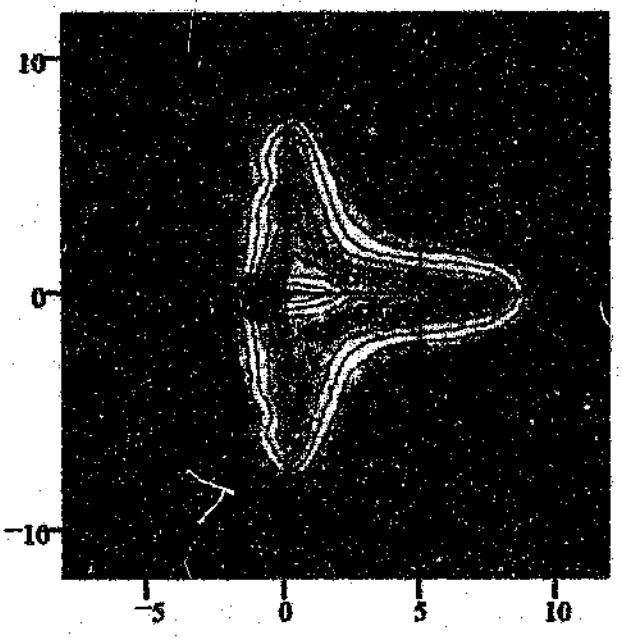


D1

**Configuration:**

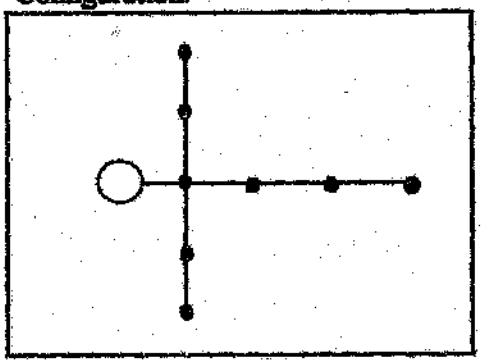

**dimensions**

| | |
|---|---|
| trench depth | 1m |
| radial length | 8m |
| rod length | 1.5m |
| number or rods | 7 |

* V = 226.5V
* I = 9.5A
∴R = 23.8Ω
* measured at the point where the earth lead enters the ground

** Rmegger = 23.1Ω
** measured using an earth resistance megger (DET5)

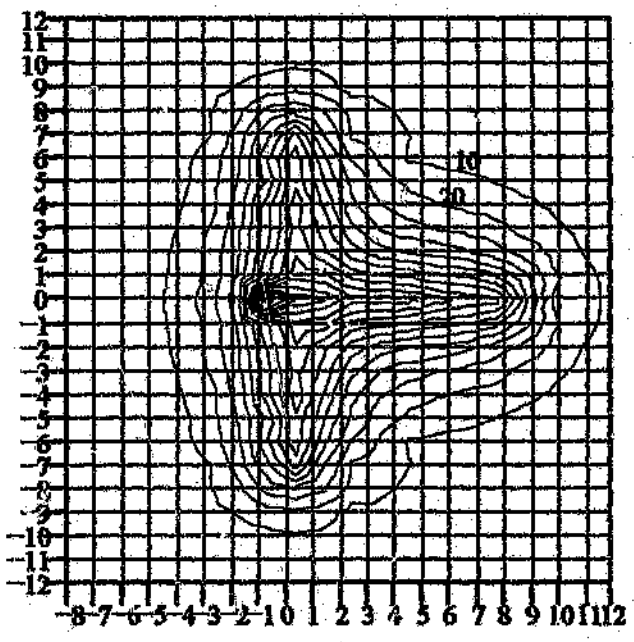


D1

**Contours**

minimum value 10V
maximum value 110V
steps of 10V

**grids**

1m x 1m

**Fig E1 : Surface equipotential for electrode E**

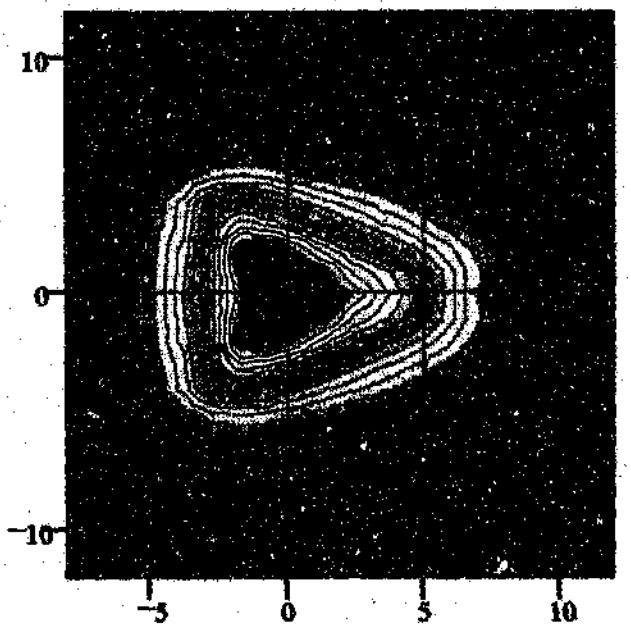


E1

**Configuration:**

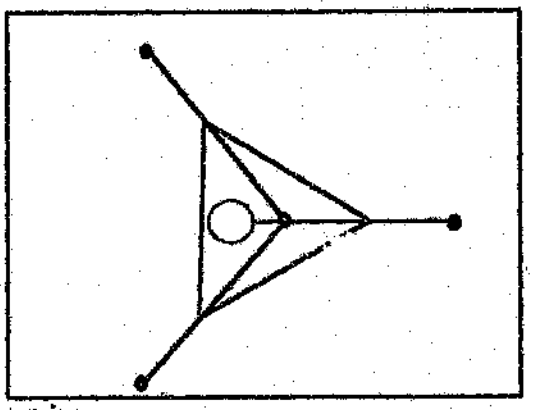

**Dimensions**

| | |
|---|---|
| trench depth | 1m |
| radial length | 6m |
| rod length | 1.5m |
| number or rods | 4 |

* V = 224V
* I = 6.2A
∴R = 36.6Ω
* measured at the point where the earth lead enters the ground

** Rmegger = 26.4Ω
** measured using an earth resistance megger (DET5)

**Contours**

minimum value 10V
maximum value 180V
steps of 10V

**grids**

1m x 1m

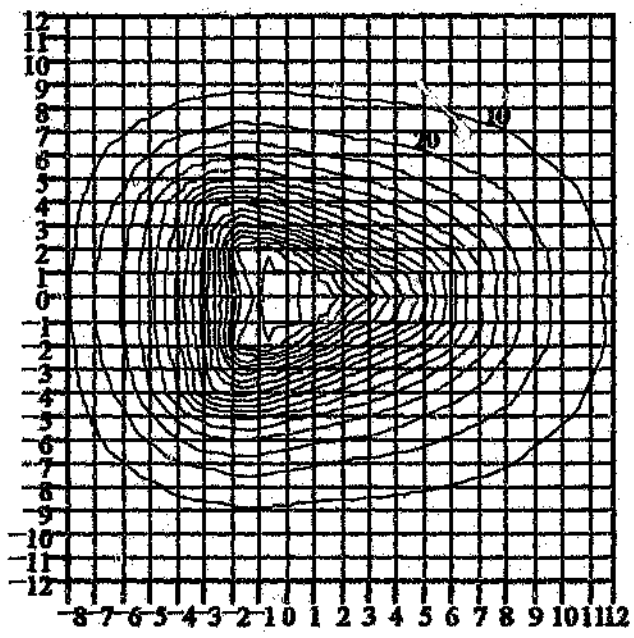


E1

Fig F1 : Surface equipotentials of electrode F

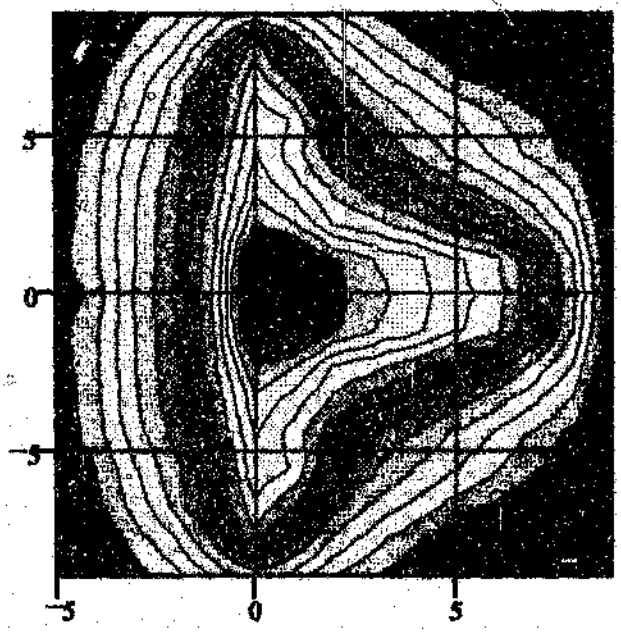


F1

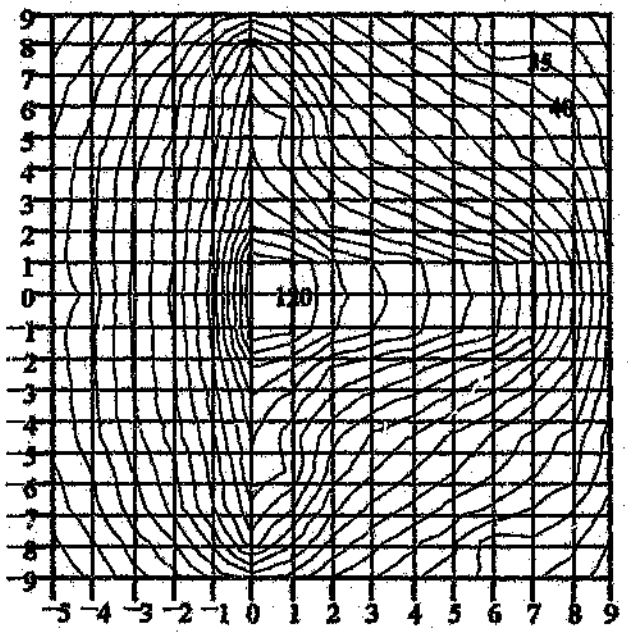


F1

Configuration:

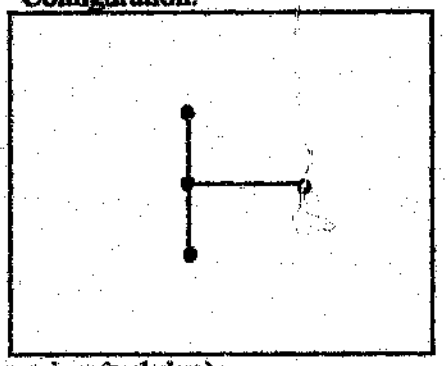

Dimensions (scaled up)

| | |
|---|---|
| trench depth | 1m |
| radial length | 6m |
| rod length | 3m |
| number or rods | 4 |

* V = 18.92V
I = 101.5mA
∴R = 186.4Ω
* measured at the point where the wire entered the water

Scaling factor = 15.4*4/8.08=7.4

Contours

minimum value 25V
maximum value 125V
steps of 5V

grids

1m x 1m
(scaled up)

Fig G1 : Surface equipotentials of electrode G

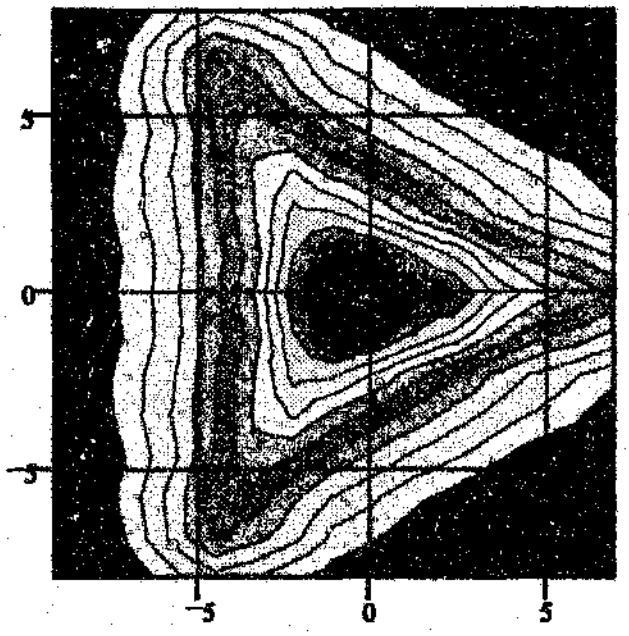


G1

Cofiguration:

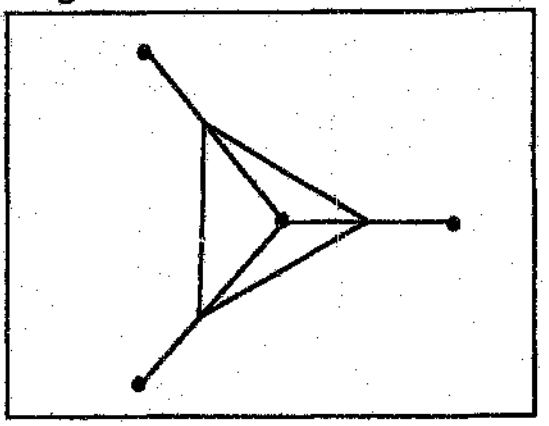

Dimensions (scaled up)

| | |
|---|---|
| trench depth | 1m |
| radial length | 6m |
| rod length | 1.5m |
| number or rods | 4 |

* V = 15.15V
I = 103.7mA
∴R = 146Ω
* measured at the point where the wire entered the water.

Scaling factor =15*5/4=18.75

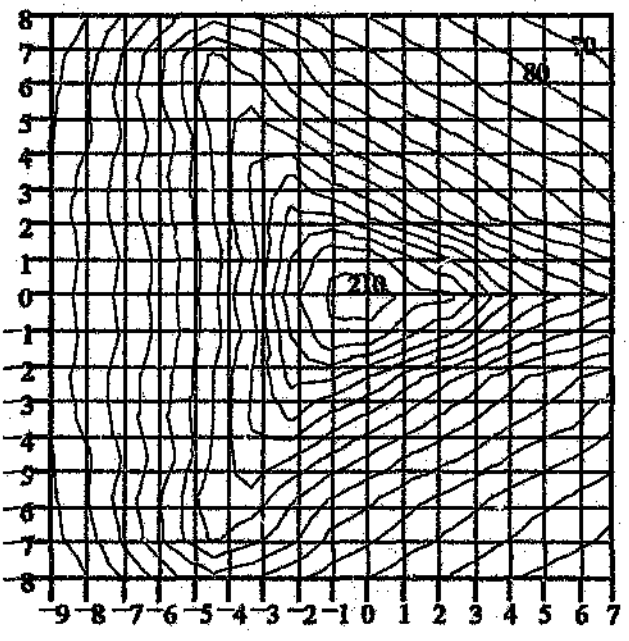


G1

Contours

minimum value 70V
maximum value210V
steps of 5V

grids

1m x 1m
(scaled up)

ROGOWSKI COILS

A Rogowski coil is an air-cored current transformer with the main current carrying conductor acting as the primary winding. The secondary winding is terminated in a passive resistor-capacitor (RC) integrator, as shown in the figure C1 below:

Fig C1 : Rogowski coil - Circuit diagram

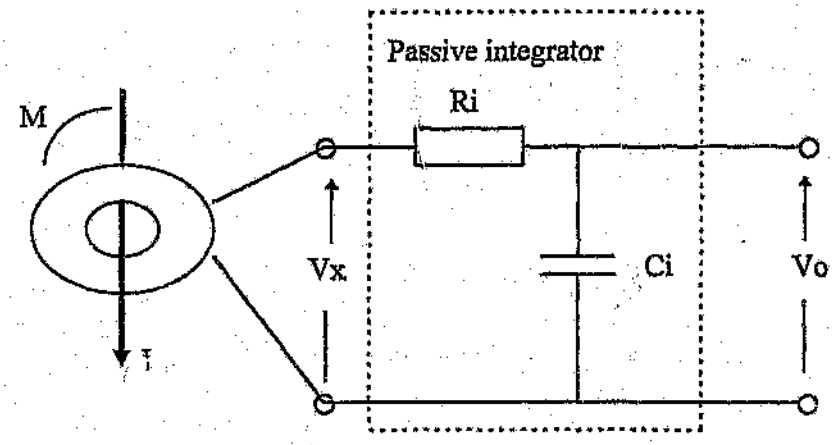


$Vx = M * dI/dt$ $\qquad Vo = \frac{M}{Ri * Ci} * I$

The advantage of using an air core is that very high currents may be measured without saturation and bandwidth problems. The limit of the system's bandwidth is determined by the RC time constant of the integrator. The period of the lowest frequency signal should be very much less than the product RC.
For the Rogowski coil used in the tests, the RC time constant was approximately 3 milliseconds - resulting in a low frequency cut-off of about 320 Hertz. A standard 8/20 microseconds current impulse is well within the required limits.

For low frequency steady-state measurements, the transfer function is determined by the mutual inductance (M) and the rate of change of primary current (dI/dt). For 50 Hertz sinusoidal current the transfer function is given by:

$$Vo/I = 2*\Pi*50*M$$

# APPENDIX D - SOIL RESISTIVITY MEASUREMENTS

GATE

# LOCATIONS OF SURVEY'S AT NEFA

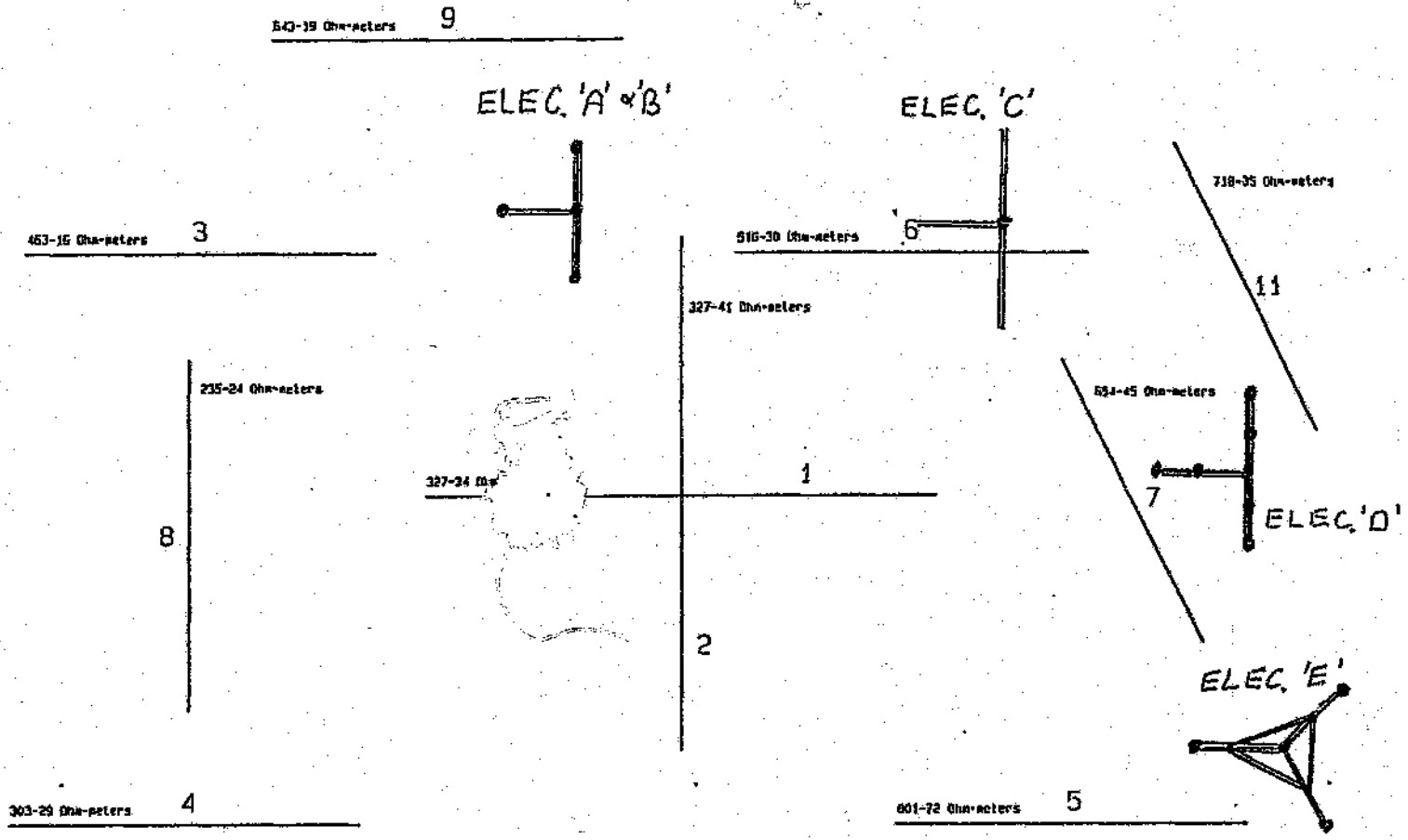


D1

# NETFA SOIL SURVEY

## Wenner Survey 1

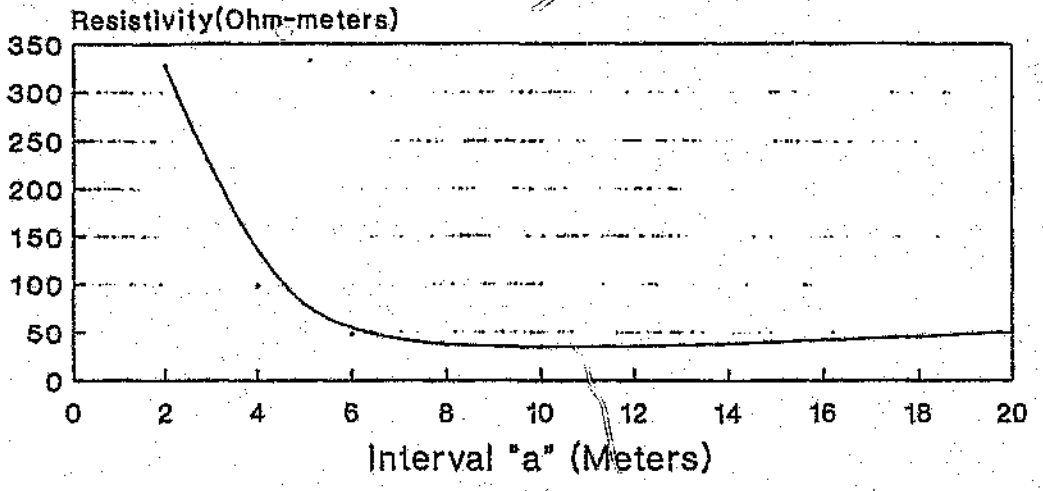


## Wenner Survey 2

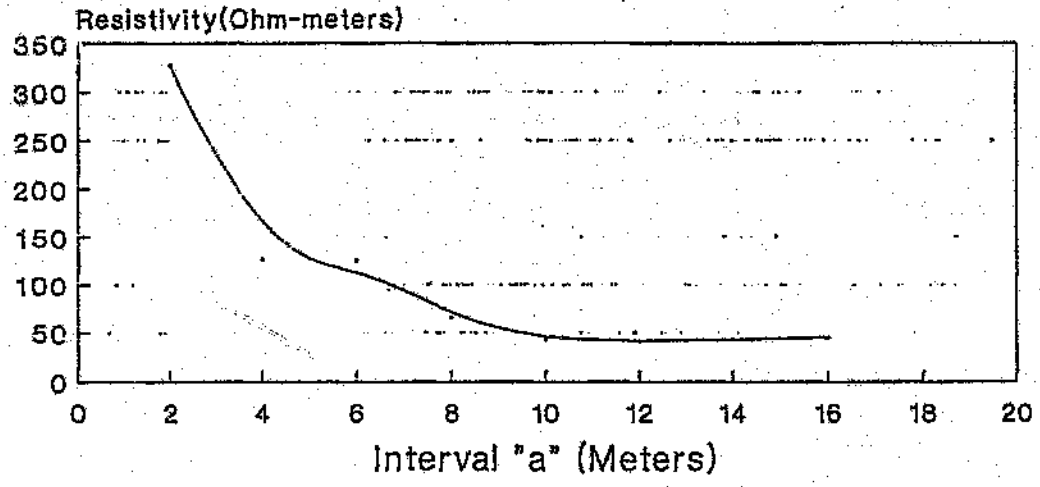


## Wenner Survey 3

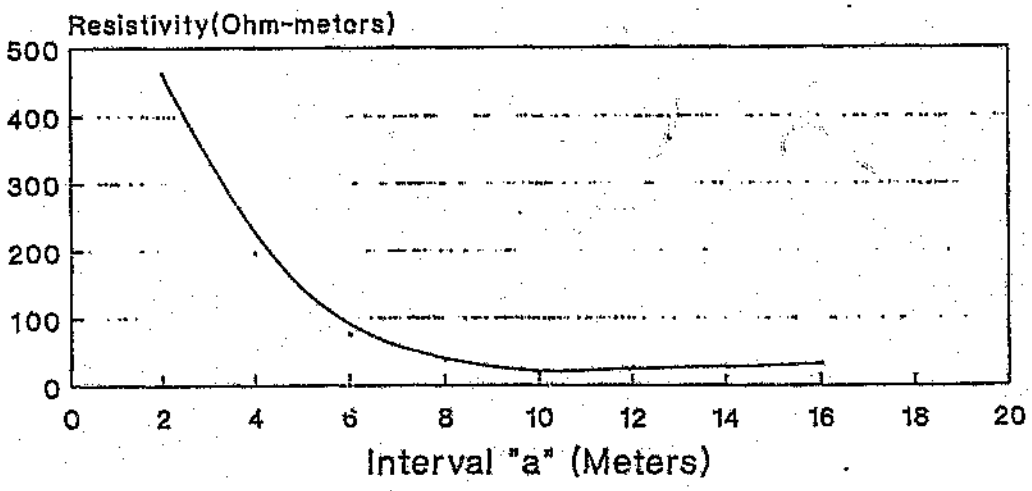


Depth=3/4x"a"

# NETFA SOIL SURVEY



## Wenner Survey 4

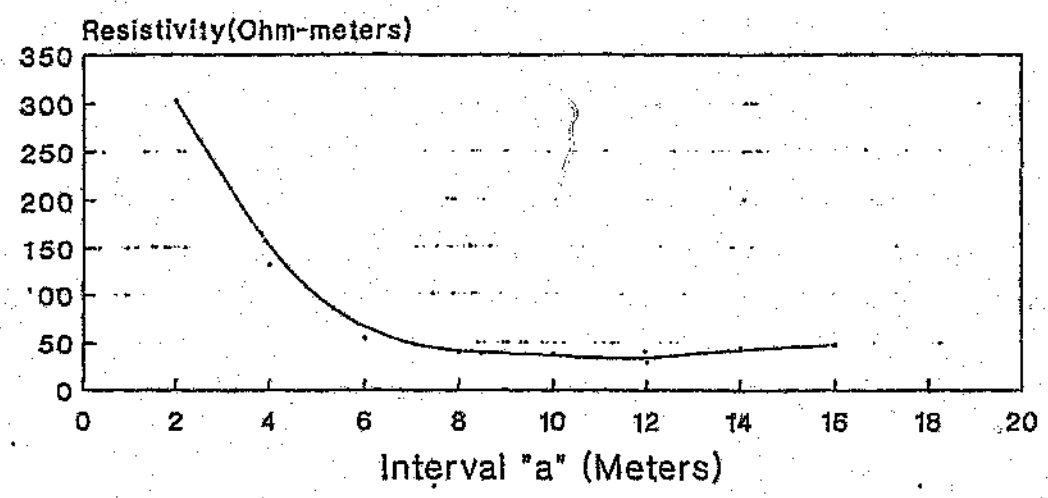


## Wenner Survey 5

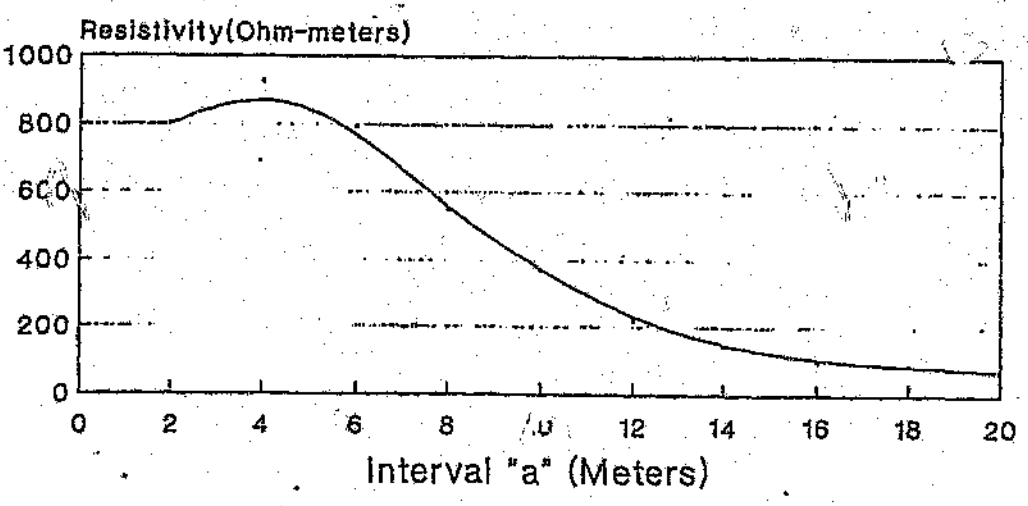


## Wenner Survey 6

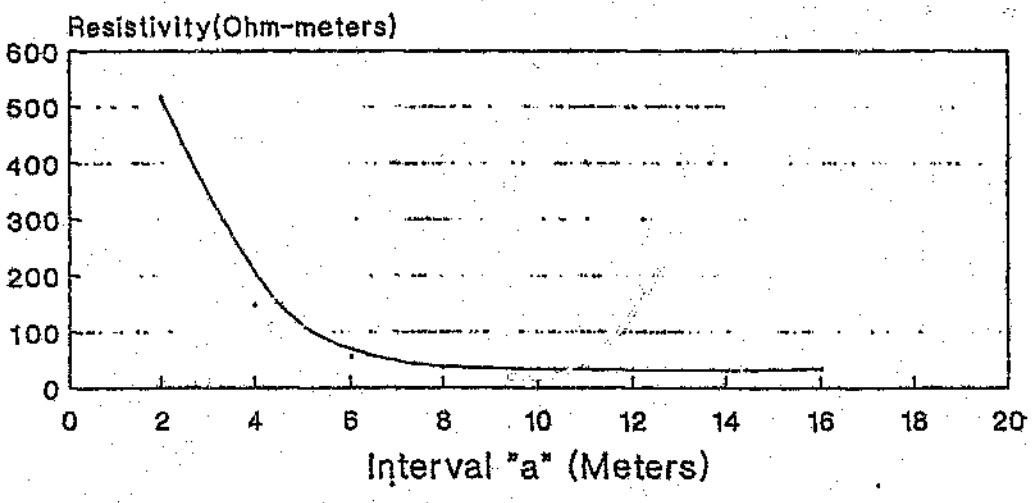


Depth=3/4x"a"

# NETFA SOIL SURVEY

D4

## Wenner Survey 7

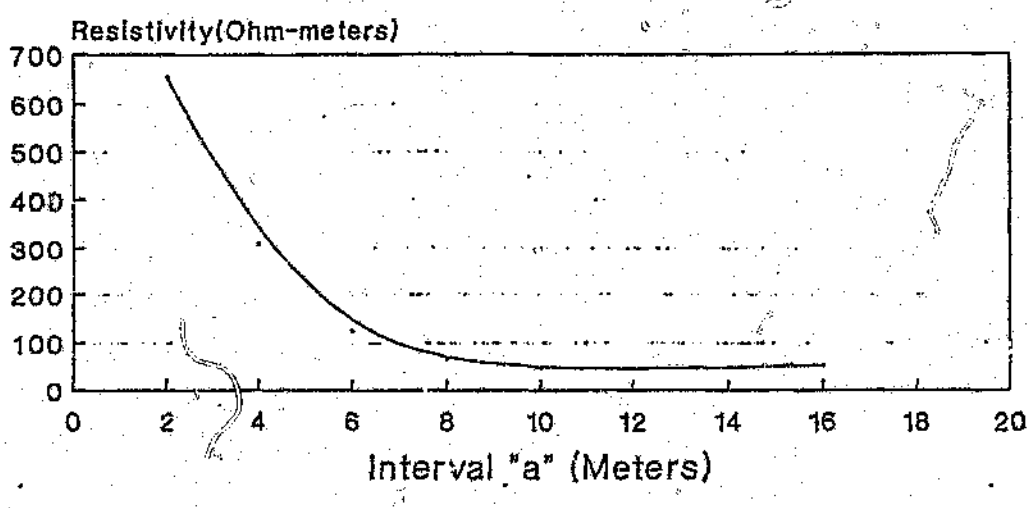


## Wenner Survey 8

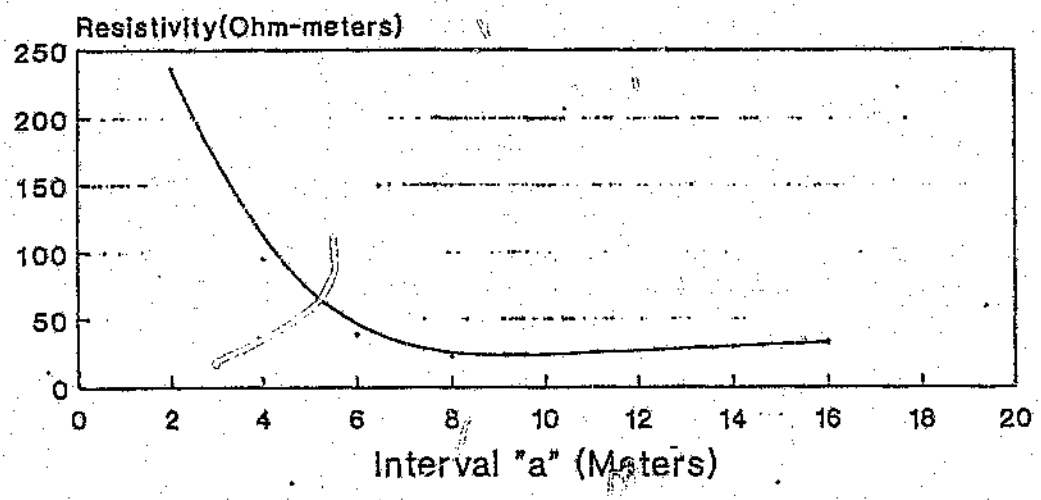


## Wenner Survey 9

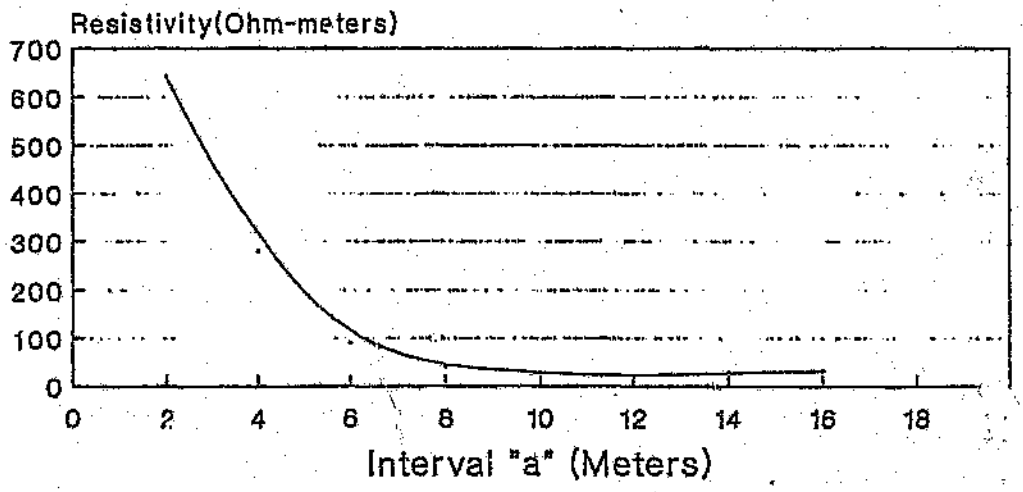


Depth=3/4x"a"

# NETFA SOIL SURVEY



## Wenner Survey 10

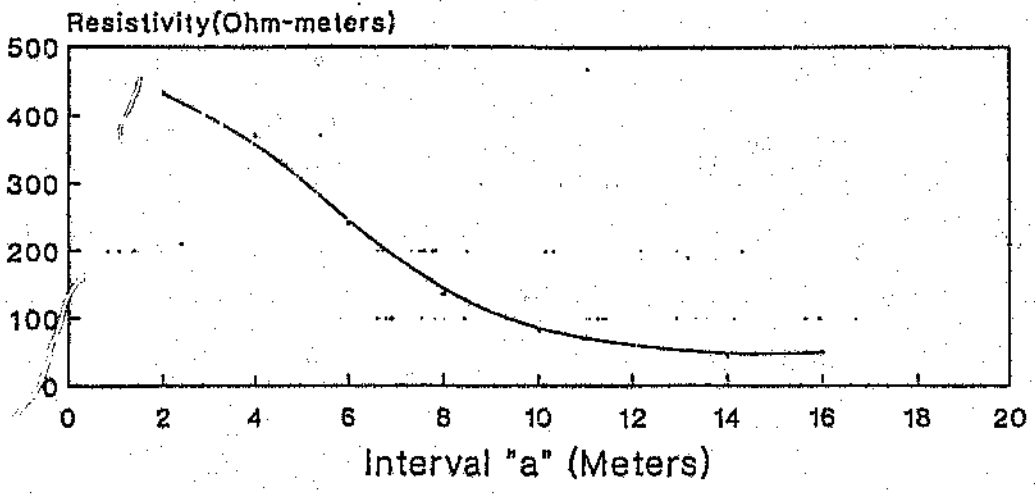


## Wenner Survey 11

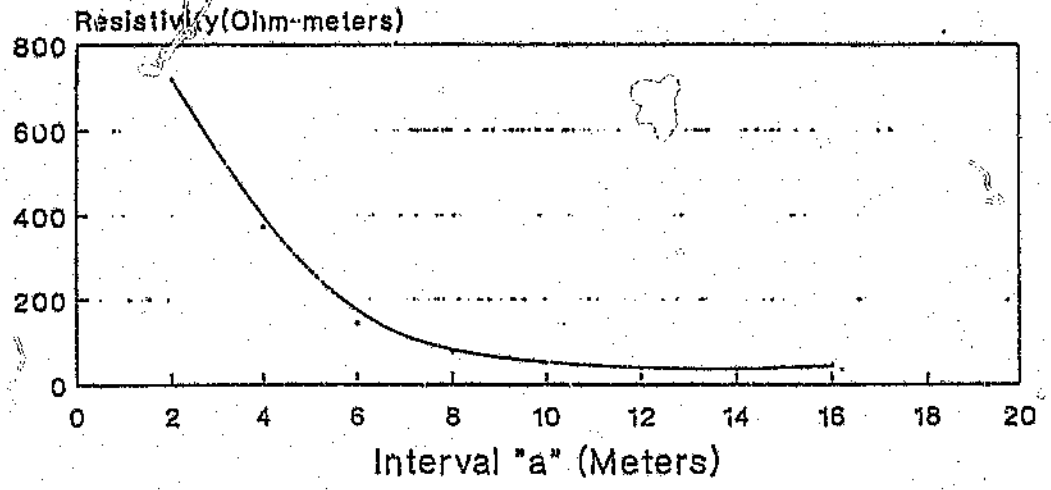


Depth=3/4x"a"

## APPENDIX E - IMPULSE TESTS RESULTS

### Electrode 'A' test

Charging voltage : 30 kV
Generator Output:

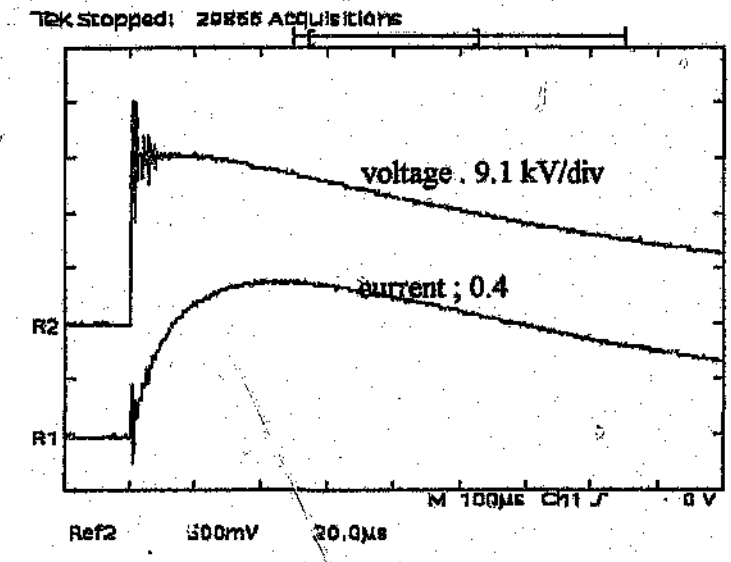


At the electrode:

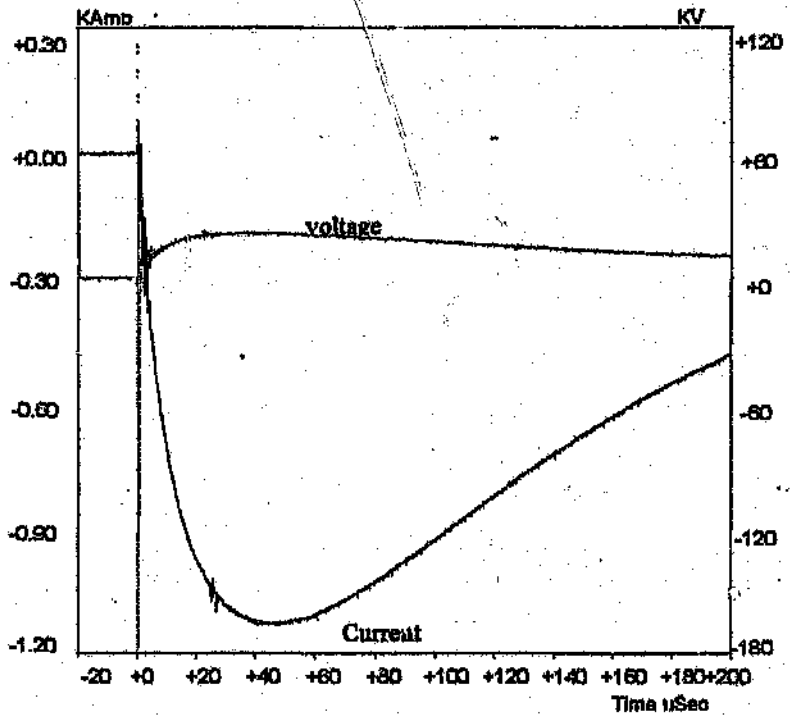

Charging voltage : 50kV
Generator output:

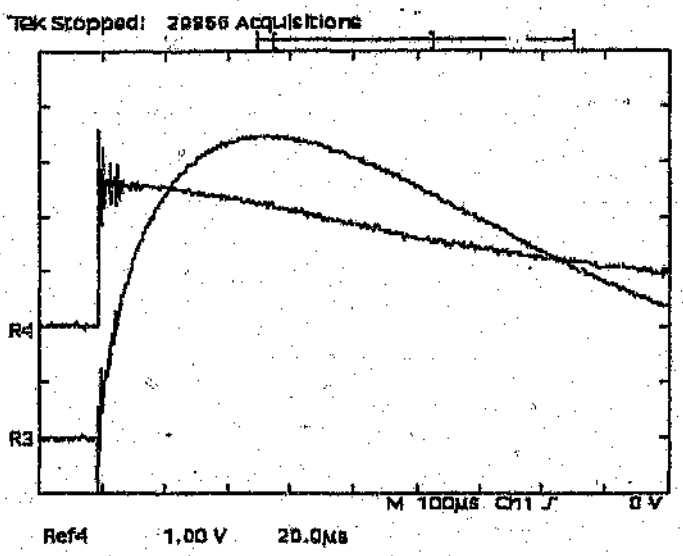


R4 : Voltage 18.3 kV / div

R3 : Current 0.4 kA / div

At the electrode:

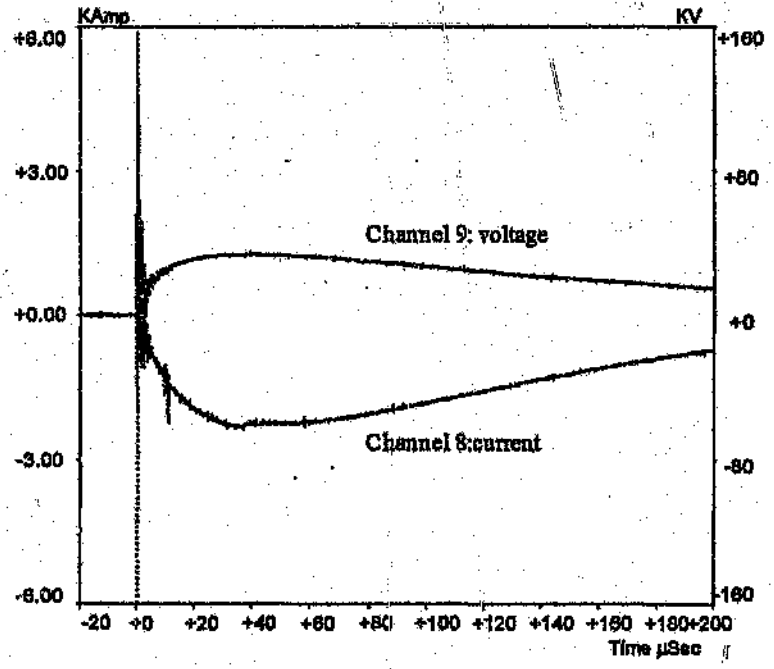

Charging voltage : 75kV
Generator output :

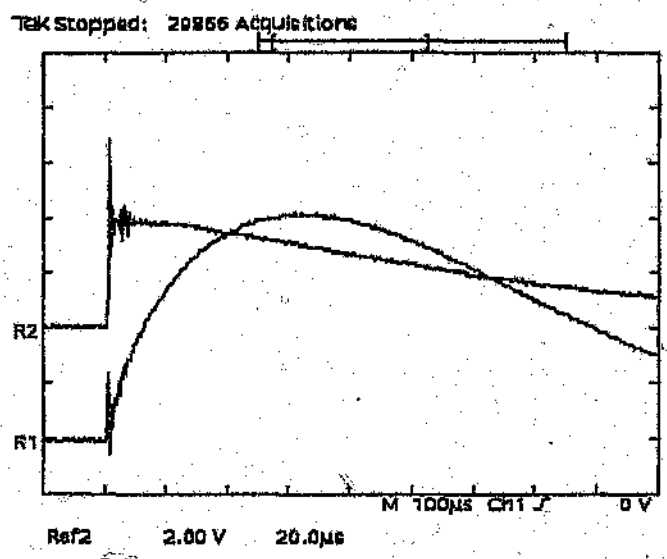


R2 : Voltage 36.5 kV / div

R3 : Current 1 kA / div

At the electrode:

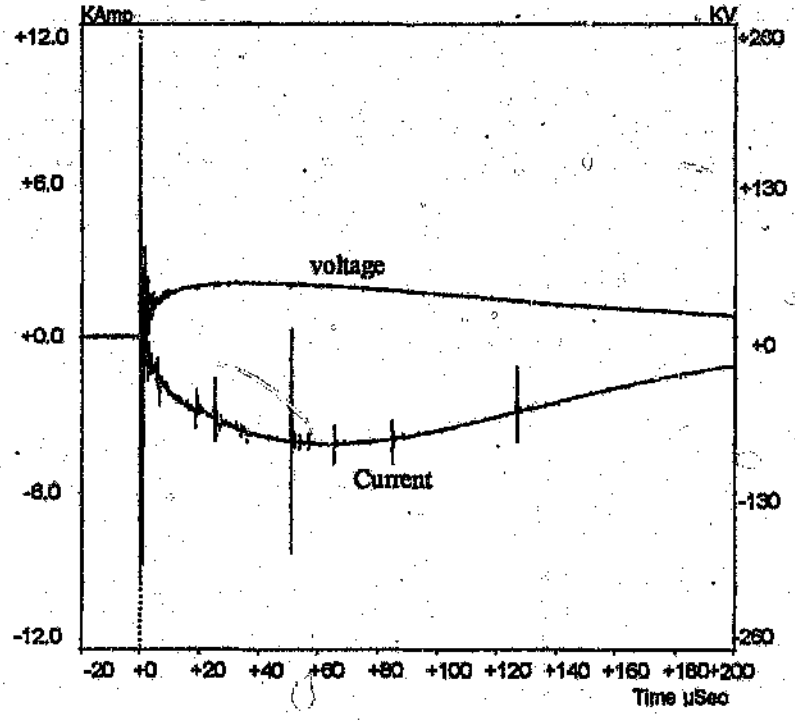

Charging voltage : 100kV

Generator output:

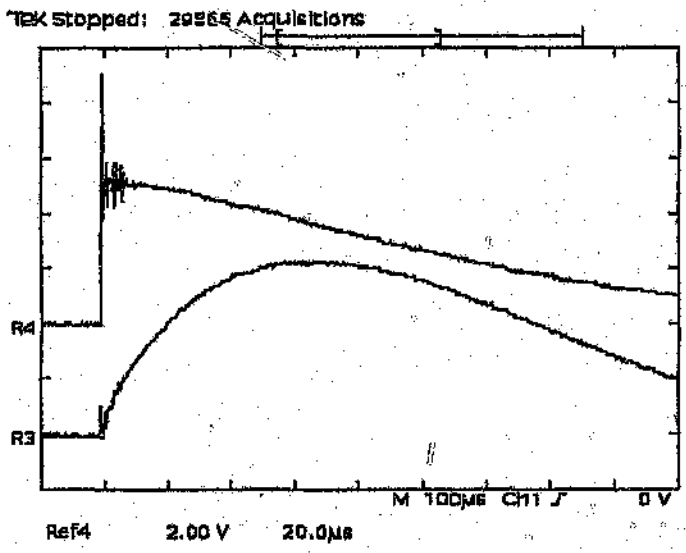


R4 : Voltage 36.5 kV / div

R3 ; Current 2 kA / div

At the electrode:

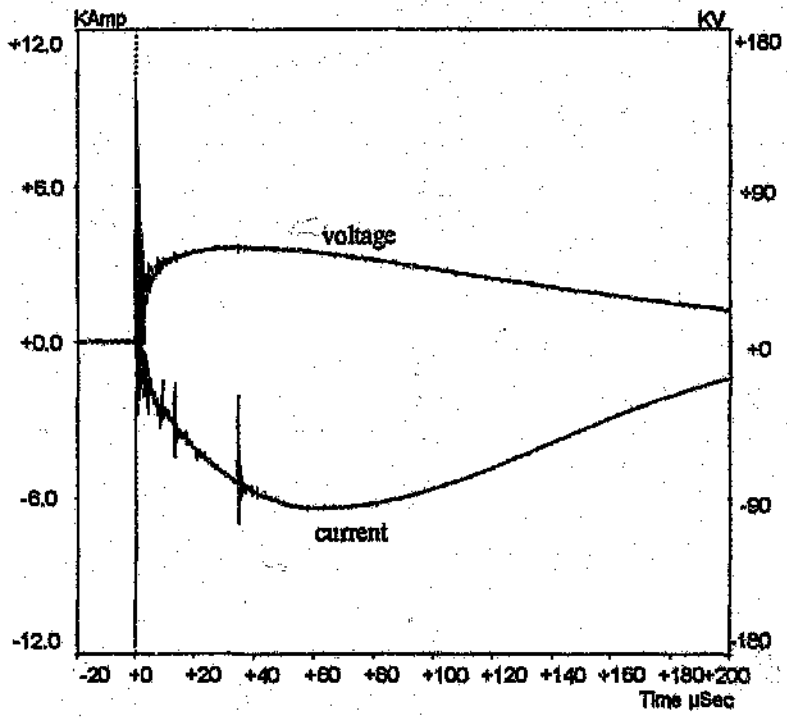

Charging voltage : 125 kV
Generator output:

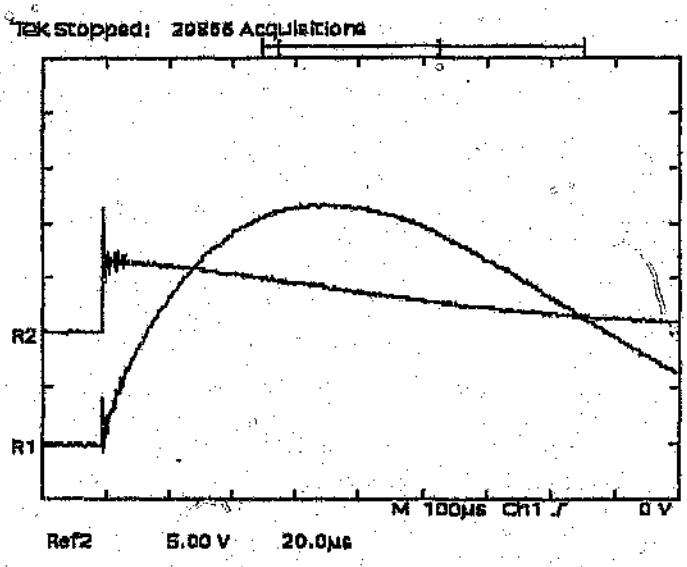


R2 : Voltage 91.3 kV / div

R1 : Current 2 kA / div

At the electrode:

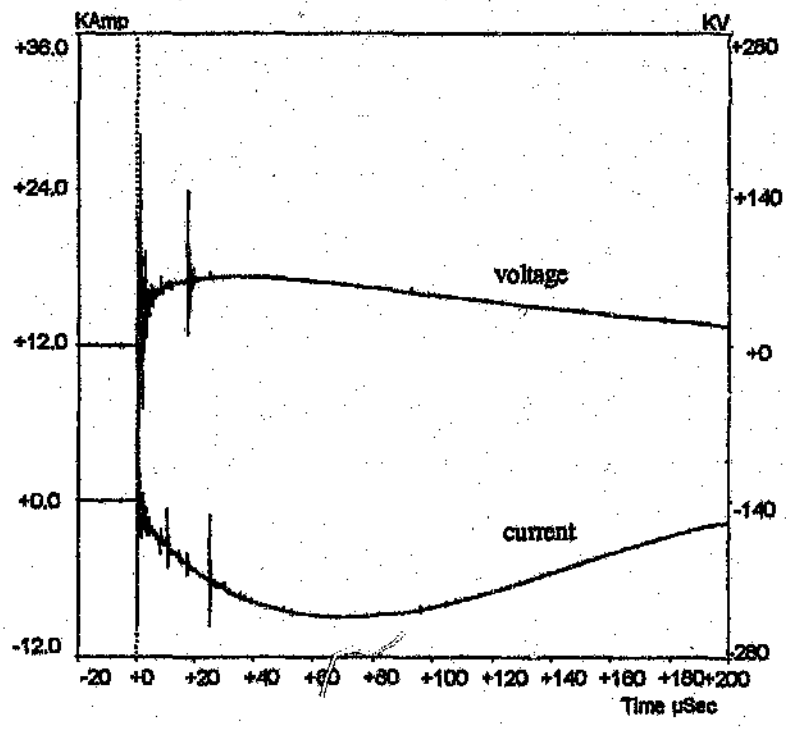

Charging voltage: 150kV

Generator output:

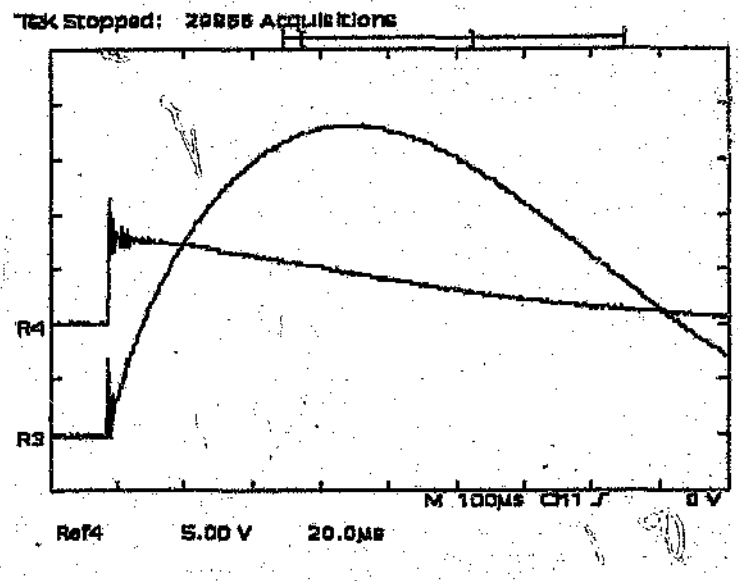


R4 : Voltage 91.3 kV / div

R3 : Current 2 kA / div

At the electrode:

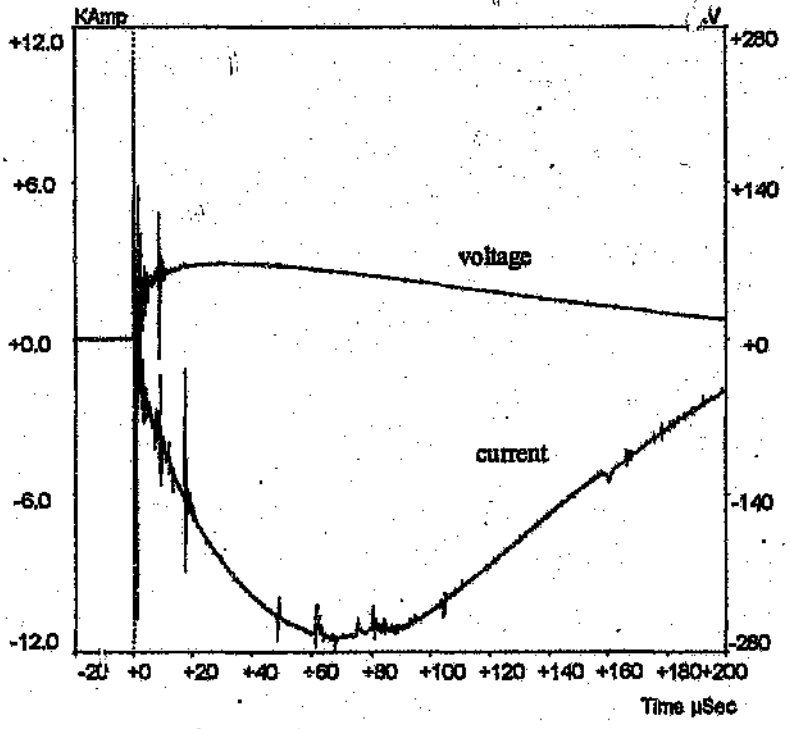

**Electrode 'B' tests**

Charging voltage : 30 kV
Generator output:

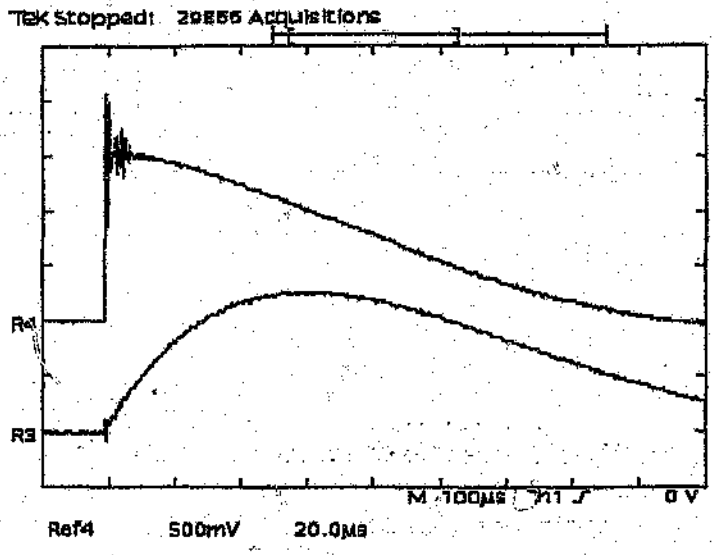


R4 : Voltage 9.1 kV / div

R3 : Current 1 kA / div

At the electrode:

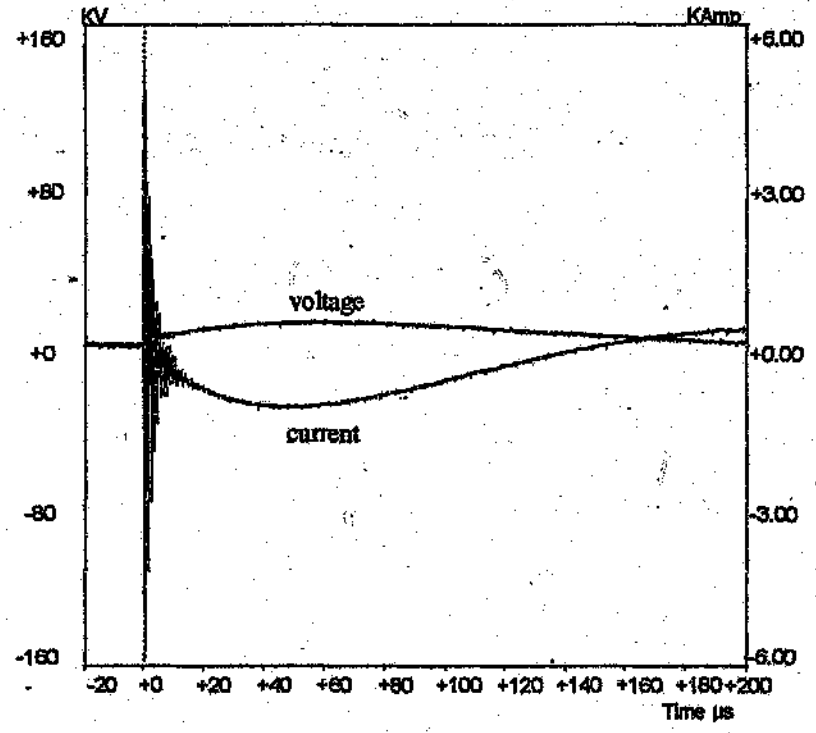

Charging voltage : 50 kV
Generator output:

At the electrode:

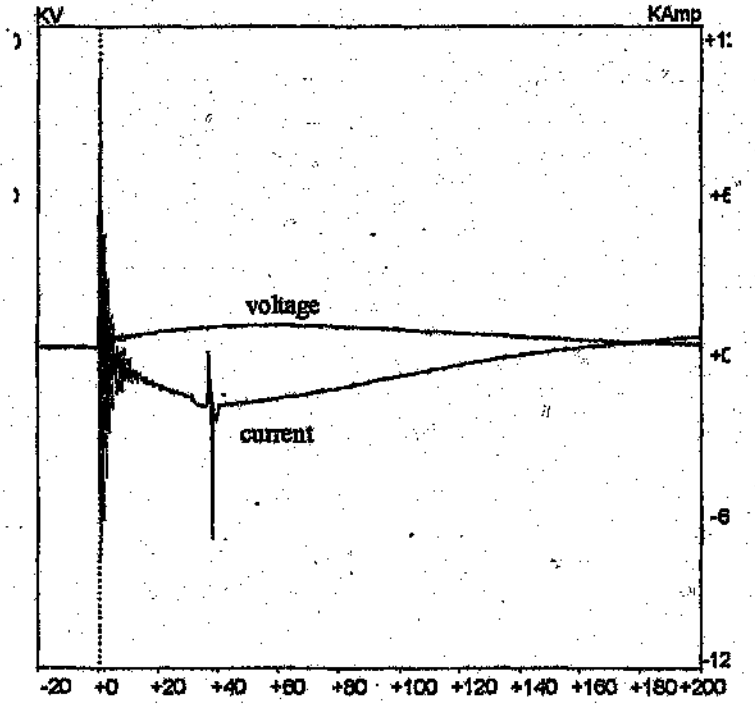

Charging voltage : 75kV
Generator output:

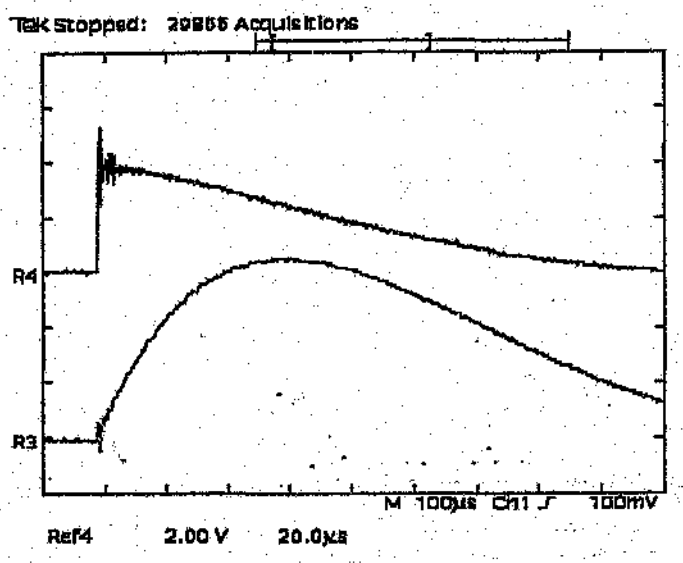


R4 : Voltage 36.5 kV / div

R3 : Current 2 kA / div

At the electrode:

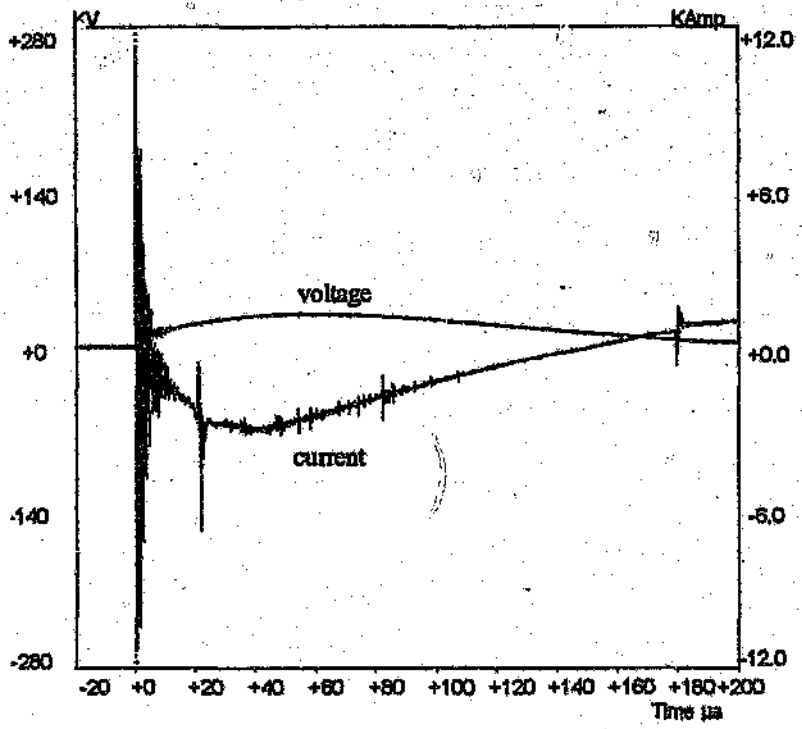

Charging voltage : 100 kV
Generator output:

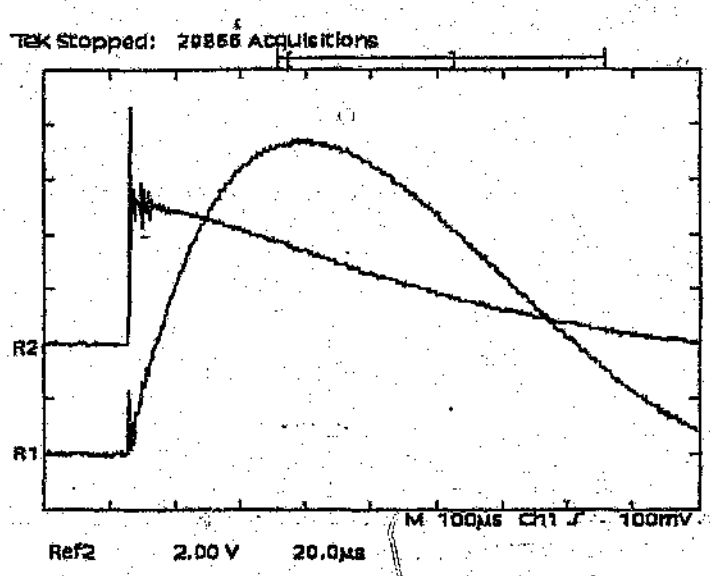


R2 : Voltage 36.5 kV / div

R1 : Current 2 kA / div

At the electrode

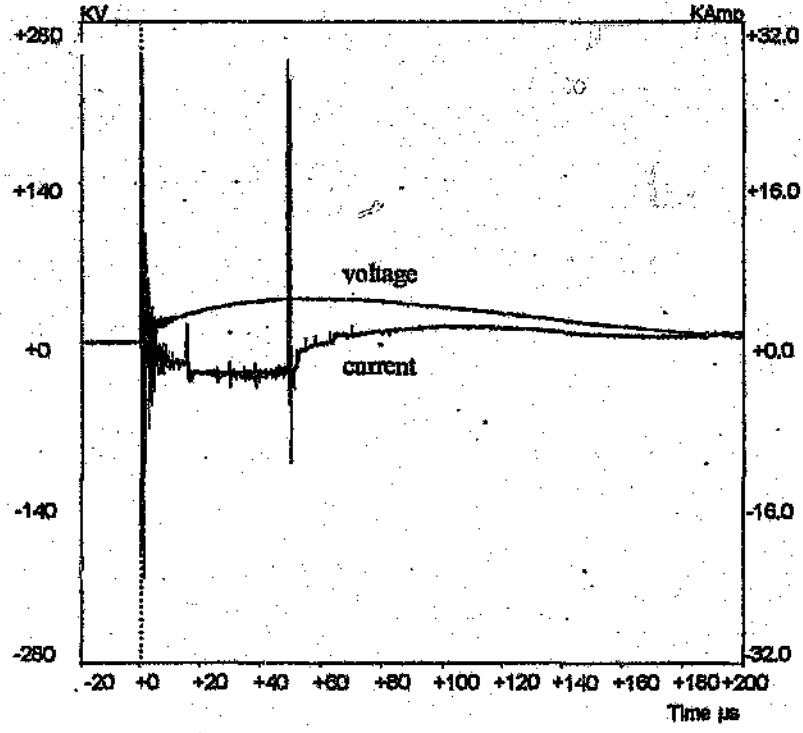

Charging voltage : 125 kV
Generator output:

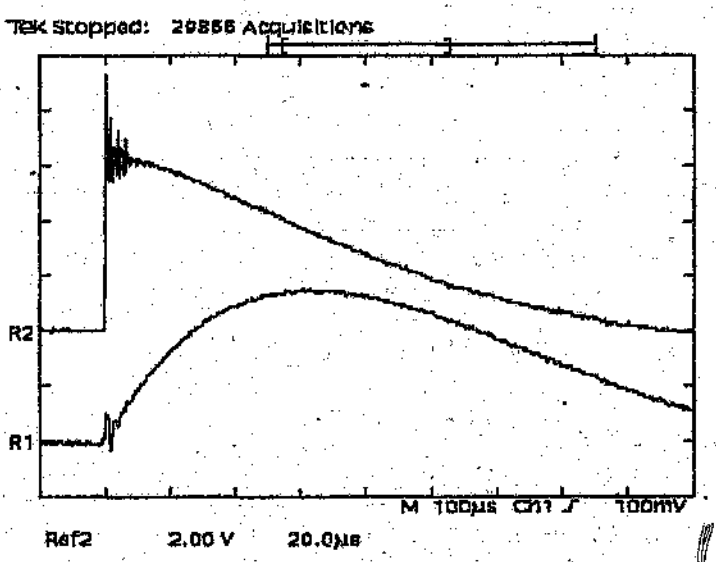


R2 : Voltage 36.5 kV / div

R1 : Current 4 kA / div

At the electrode

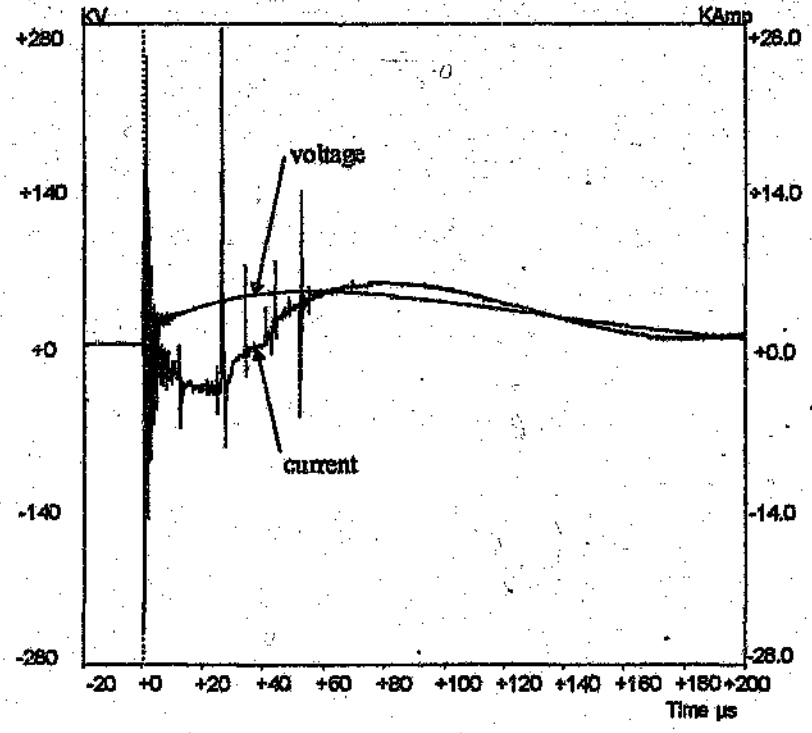

Charging voltage : 150 kV
Generator output:

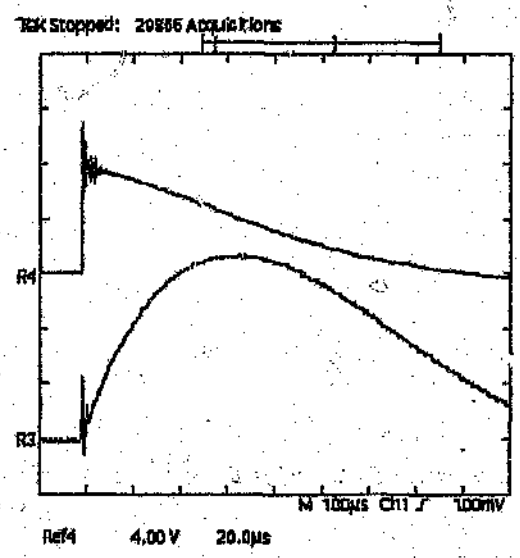


R4 : Voltage 73 kV / div

R3 : Current 4 kA / div

1. IEEE Guide for Safety in AC Substation Grounding. ANSI/IEEE std 80-1986.

2. Substation Grounding Scale Model Tests. EPRI project 1494-3 Interim report May 1983.

3. Caldecott R. and Kasten D.G. , Scale Model Studies of Station Grounding Grids, IEEE Trans. Vol. PAS-102, No. 3, 1983.

4. Thapar B. and Puri K.K. , Mesh Potentials in High-Voltage Grounding Grids, IEEE Trans. Vol. PAS-86, No. 2, 1967.

5. Blattner C.J. , Prediction of soil resistivity and Ground Rods Resistance for Deep Ground Electrodes, IEEE Trans. Vol. PAS-99, No. 5, 1980.

6. Takahashi T. and Kawase T. , Calculation of Earth Resistances for deep Driven Rods in Multi-layer Earth Structure, IEEE Trans. on Power Delivery, Vol 6, No. 2, 1991.

7. Liew A.C. and Darveniza M. , Dynamic Model of Impulse Characteristic of Concentrated Earths , IEE Proc. Vol 121, No. 2 , 1974.

8. Mazzetti C. and Veca G.M. , Impulse Behaviour of Ground Electrodes, IEEE Trans. Vol PAS-102, No. 9 , 1983.

9. Velazquez R. and Mukhedkar D. , Analytical Modelling of Grounding Electrodes Transient Behaviour, IEEE Trans. Vol PAS-103, No. 6, 1984.

10. Oettle E.E. , The Characteristics of Electrical Breakdown and Ionization Processes in Soil, SAIEE Trans. 1988.

11. Oettle E.E. and Geldenhuys H.J. , Results of Impulse Tests on Practical Electrodes at the High Voltage Laboratory of the National Electrical Engineering Research Institute, SAIEE Trans. 1988.

12. Chisholm W.A. and Janischewskyj W. , Lightning Surge Respone of Ground Electrodes, IEEE Trans. on Power Delivery, Vol 4, No. 2 , 1989.

13. Cattaneo S. et Al, Transient Behaviour of Grounding Systems Simulation: Remarks on EMTP and special codes used. EMTP Trans 1993.

14. Meliopoulos Sakis A.P. , Power System Grounding and Transients, Marcel Dekker Inc. 1988.

15. Analysis Techniques for Substation Grounding Systems, EPRI final report EL-2682, Vol 1 and 2 , 1982.

16. Dawalibi F. and Mukhedkar D. , Optimum Design of Substation Grounding in Two Layer Earth Structure, IEEE Trans Vol PAS-94, No. 2, 1975.

17. Bellashi P.L. , Impulse and 60-Cycle Characteristics of Driven Grounds, Trans AIEE, Vol 60, 1941.

18. Bellashi P.L. Armington R.E. and Snowden A.E., Impulse and 60-Cycle Characteristics of Driven Grounds, Trans AIEE, Vol 61, 1942.

19. Petropoulos G.M. , The High Voltage Characteristics of Earth Resistances, J. IEE, Vol 95 part II, 1948.